UNIVERSIDADE ESTADUAL PAULISTA
"JÚLIO DE MESQUITA FILHO"
CAMPUS PRESIDENTE PRUDENTE
FACULDADE DE CIÊNCIAS E TECNOLOGIA
Programa de Pós-Graduação em Ciências Cartográficas

CAROLINE PIFFER DE ANDRADE

REMOTE SENSING OF CHLOROPHYLL-*A* CONCENTRATION BASED ON ABSORPTION COEFFICIENTS IN IBITINGA RESERVOIR

PRESIDENTE PRUDENTE
2018

CAROLINE PIFFER DE ANDRADE

REMOTE SENSING OF CHLOROPHYLL-*A* CONCENTRATION BASED ON ABSORPTION COEFFICIENTS IN IBITINGA RESERVOIR

A dissertation submitted to the Faculty of Science and Technology of São Paulo State University in partial fulfillment of the requirements for the degree of Master of Cartographic Sciences.

Advisor: Prof. Dr. Enner Alcântara
Co-advisor: Dr. Milton Kampel

PRESIDENTE PRUDENTE
2018

Ficha catalográfica elaborada pela Seção Técnica de Aquisição e Tratamento da Informação - Diretoria Técnica de Biblioteca e Documentação - UNESP, Campus de Presidente Prudente

Piffer de Andrade, Caroline.
A566r Remote sensing of chlorophyll-*a* concentration based on absorption coefficients in Ibitinga reservoir / Caroline Piffer de Andrade. - 2018
65 f. : il.

Orientador: Enner Herenio de Alcântara
Dissertação (mestrado) - Universidade Estadual Paulista. Faculdade de Ciências e Tecnologia, Presidente Prudente, 2018
Inclui bibliografia

1. Qualidade de águas interiores. 2. Algoritmo quase-analítico. 3. Propriedades óticas inerentes. I. Herenio de Alcântara, Enner. II. Universidade Estadual Paulista. Faculdade de Ciências e Tecnologia. III. Título.

Alessandra Kuba Oshiro Assunção
CRB-8/9013

unesp

UNIVERSIDADE ESTADUAL PAULISTA

Câmpus de Presidente Prudente

CERTIFICADO DE APROVAÇÃO

TÍTULO DA DISSERTAÇÃO: REMOTE SENSING OF CHLOROPHYLL-A CONCENTRATION BASED ON ABSORPTION COEFFICIENTS IN IBITINGA RESERVOIR

AUTORA: CAROLINE PIFFER DE ANDRADE
ORIENTADOR: ENNER HERENIO DE ALCÂNTARA
COORIENTADOR: MILTON KAMPEL

Aprovada como parte das exigências para obtenção do Título de Mestra em CIÊNCIAS CARTOGRÁFICAS, área: AQUISIÇÃO, ANÁLISE E REPRESENTAÇÃO DE INFORMAÇOES ESPACIAIS pela Comissão Examinadora:

Prof. Dr. ENNER HERENIO DE ALCÂNTARA
Departamento de Engenharia Ambiental / Instituto de Ciência e Tecnologia de São José dos Campos

Profa. Dra. THANAN WALESZA PEQUENO RODRIGUES GUIMARÃES
IFPA / Instituto Federal do Pará

Dr. LUIZ HENRIQUE DA SILVA ROTTA
Pós-doutorando PNPD / Faculdade de Ciencias e Tecnologia de Presidente Prudente

Presidente Prudente, 23 de março de 2018

To my parents, Alessandra e Paulo

AGRADECIMENTOS

Agradeço a todos que, de alguma forma, colaboraram com este trabalho.

Meus agradecimentos especiais:

À Força Divina, que tem me guiado ao longo de todas as etapas de minha vida.

Aos meus pais, Alessandra e Paulo, por todo apoio, incentivo, amor e pelos sacrifícios que sempre fizeram para que eu pudesse seguir os meus sonhos.

Ao meu padrasto e madrasta, Fábio e Renata, pelo incentivo e amizade.

Aos meus irmãos, João Pedro e Tiago, pela amizade de sempre.

Aos meus avós, Maria Aparecida, Darcy e Líbera, que mesmo diante de situações desfavoráveis sempre nos ensinaram que a educação é prioridade.

Ao meu companheiro da vida, Henrique, por todo amor, apoio e por ser o meu maior incentivador.

Ao meu orientador, Prof. Enner Alcântara, agradeço pelos ensinamentos e por sempre exigir o meu melhor. Muito obrigada por todo o apoio e principalmente pela confiança.

Ao meu co-orientador, Dr. Milton Kampel, por toda ajuda e confiança neste trabalho.

Aos professores do Programa de Pós-Graduação em Ciências Cartográficas, pelo conhecimento compartilhado.

Aos amigos e colegas do Programa de Pós-Graduação, especialmente:

Carol Campos, Bruno Faga, Carol Ambrósio, Sarah Martins, Nariane Bernando, Alisson Carmo, Fernanda Watanabe, Luiz Rotta e Thanan Guimarães.

Aos membros da banca, por aceitarem avaliar e contribuir com este trabalho.

À FCT-UNESP pela infraestrutura que possibilitou a realização desse trabalho.

Aos funcionários da UNESP, em especial da Seção de Pós-Graduação e à Cidinha e Zilda, por todas as palavras de carinho e incentivo.

Ao Prof. Edivaldo Velini (FCA/UNESP) e funcionários do Laboratório de Matologia, pela disponibilização do laboratório.

À **FAPESP** (Fundação de Amparo à Pesquisa do Estado de São Paulo) pelo financiamento de projetos (**Processos N° 2012/19821-1** e **2015/21586-9**).

À **CAPES/MEC** (Coordenação de Aperfeiçoamento de Pessoal de Nível Superior – Ministério da Educação) pela bolsa de mestrado.

A todos, meu muito obrigado!

“You cannot get through a single day without having an impact on the world around you. What you do makes a difference, and you have to decide what kind of difference you want to make.”

Jane Goodall

RESUMO

O presente estudo objetivou estimar as concentrações de clorofila-*a* (Chl-*a*) no reservatório da usina hidroelétrica de Ibitinga (RHI), localizado no Rio Tietê, estado de São Paulo, Brasil, por meio de coeficientes de absorção obtidos via algoritmos quase-analíticos (QAAs). Para isso, realizou-se uma caracterização bio-ótica e biogeoquímica do RHI, por meio de dados espectrais e de qualidade da água coletados em dois trabalhos de campo, conduzidos em Julho de 2016 e Junho de 2017. Os desempenhos das versões originais QAA_{V5} e QAA_{V6} em estimar as propriedades óticas inerentes (POIs) no RHI foram avaliados. Versões re-parametrizadas para dois reservatórios localizados no sistema em cascata do Rio Tietê, QAA_{BBHR} e QAA_{OMW}, foram também testadas para a área de estudo. Além disso, foram avaliadas as performances de esquemas compostos pelas versões do QAA já mencionadas, seguidas por quatro modelos para estimativa de Chl-*a*, os quais utilizam coeficientes de absorção como dados de entrada. A distribuição espacial das concentrações de Chl-*a* foi analisada por meio da aplicação desses esquemas em uma imagem do sensor *Ocean and Land Colour Instrument* (OLCI) instalado a bordo do satélite Sentinel-3A, com aquisição coincidente com o segundo trabalho de campo realizado na área de estudo. A caracterização bio-ótica demonstrou variabilidade espacial e temporal dos constituintes oticamente significativos (COSs) no RHI, com predominância da absorção pelo material orgânico colorido dissolvido (CDOM). As versões do QAA testadas para o primeiro conjunto de dados não se mostraram completamente adequadas na obtenção de coeficientes de absorção em todos os comprimentos de onda. Com relação aos esquemas para estimativa de concentração de Chl-*a*, apenas aqueles baseados no QAA_{V5} foram capazes de obter resultados razoáveis - Raiz do Erro Médio Quadrático Normalizado (REMQN) < 47.50 % - para os dados da imagem OLCI. Todos os quatro modelos para estimativa de Chl-*a* testados apresentaram resultados similares para os dados de saída do QAA_{V5}. Esses resultados enfatizam o desafio gerado pela grande variabilidade ótica dos sistemas em cascata, com relação à modelagem bio-óptica. Os resultados obtidos dão suporte a futuros trabalhos, os quais podem resultar em aplicações como o monitoramento do estado trófico na área de estudo a partir de dados de satélite, com maior acurácia proveniente do uso de modelos que possam estimar consistentemente suas POIs.

Palavras-chave: Qualidade de águas interiores, Algoritmo Quase-analítico, Propriedades Óticas Inerentes, Fitoplâncton, OLCI/Sentinel-3A.

ABSTRACT

This research was aimed at retrieving chlorophyll-*a* (Chl-*a*) concentrations in Ibitinga Hydroelectric Reservoir (IHR), located at Tietê River, São Paulo State, Brazil, using absorption coefficients obtained via Quasi-analytical algorithms (QAAs). For this purpose, a bio-optical and bio-geochemical characterization of IHR was carried out, through spectral and water quality data collected in two field campaigns conducted in July, 2016 and June, 2017. The suitability of two QAA native forms (QAA_{V5} and QAA_{V6}) in retrieving inherent optical properties (IOPs) in IHR was assessed. Versions re-parameterized for two reservoirs also located in the Tietê River cascading system, QAA_{BBHR} and QAA_{OMW}, were also tested for the study area. Besides that, the performances of schemes composed by the QAA versions already mentioned followed by four models that use absorption coefficients as inputs for estimating Chl-*a* concentration in Ibitinga Reservoir were evaluated. Spatial distribution of Chl-*a* in the reservoir was analyzed, since these schemes were applied in an image of the Ocean and Land Colour Instrument (OLCI) sensor onboard Sentinel-3A satellite, with acquisition date coincident with the second field campaign. The bio-optical characterization showed spatial and temporal variability of optically significant constituent (OSC) in IHR and colored dissolved organic matter (CDOM) predominance in its absorption budget. None of the QAA versions tested for the first dataset was completely satisfactory in retrieving absorption coefficients for IHR in all wavelengths. Regarding the schemes for Chl-*a* concentration estimates, only the ones based on QAA_{V5} were able to obtain reasonable results - Normalized Root Mean Square Error (nRMSE) < 47.50 % - for the OLCI image data. All four models for Chl-*a* estimation tested presented similar results for QAA_{V5} outputs. These results highlight the challenge of copying with high optical variability in cascading systems. The results obtained support further works, which can, prospectively, lead to many practical applications, as monitoring of trophic state in the study area from satellite data, with higher accuracy provided by the use of models that can consistently retrieve the IOPs for this specific water system.

Keywords: Inland water quality, Quasi-Analytical Algorithm, Inherent Optical Properties, Phytoplankton, OLCI/Sentinel-3A.

LIST OF FIGURES

LIST OF TABLES

LIST OF ABBREVIATIONS AND ACRONYMS

BBHR	Barra Bonita Hydroelectric Reservoir
CDOM	Colored Dissolved Organic Matter
CETESB	Companhia Ambiental do Estado de São Paulo
Chl-*a*	Chlorophyll-*a*
CRCC	Cascading Reservoir Continuum Concept
C2RCC	Case-2 Regional/Coast Colour
CV	Coefficient of variation
EL	Empirical Line
ESA	European Space Agency
IHR	Ibitinga Hydroelectric Reservoir
IOPs	Inherent optical properties
ISM	Inorganic suspended matter
MAPE	Mean absolute percentage error
NDCI	Normalized Difference Chlorophyll Index
NHR	Nova Avanhandava Hydroelectric Reservoir
NIR	Near infrared
nRMSE	Normalized root mean square error
NTU	Nephelometric Turbidity Units
OD	Optical density
OLCI	Ocean Land Colour Instrument
OSC	Optically Significant Constituents
OSM	Organic suspended matter
QAA	Quasi-analytical algorithm
S3	Sentinel-3A
SD	Standard deviation
SPM	Suspended particulate matter
TOA	Top of atmosphere

LIST OF SYMBOLS

a_t	Total absorption coefficient
a_{CDOM}	Colored dissolved organic matter absorption coefficient
a_{CDM}	Colored dissolved organic matter plus detritus absorption coefficient
a_d	Detritus absorption coefficient
a_ϕ	Absorption coefficient of phytoplankton pigments
a_p	Particulate absorption coefficient
a_w	Pure water absorption coefficient
b_{bp}	Backscattering coefficient of suspended particles
b_{bw}	Backscattering coefficient of pure water
$E_d(\lambda)$	Downwelling irradiance
$F(\theta)$	Surface Fresnel reflectance
$L_r(\lambda)$	Surface-reflected radiance
$L_s(\lambda)$	Atmospheric diffuse radiance
$L_t(\lambda)$	Total upwelling radiance
R	Irradiance reflectance
R_{rs}	Remote sensing reflectance
S_{rs}	Sky remote sensing reflectance
T_{rs}	Total remote sensing reflectance
ε	Absolute percentage difference
θ	Zenith angle
ϕ	Azimuth angle
λ	Wavelength
λ_0	Reference wavelength

CONTENTS

CHAPTER 1: INTRODUCTION

1.1.Contextualization

Inland waters play a crucial role in hydrological, carbon and nutrient cycles, offer numerous ecosystem services and provide resources for multiple uses (AYRES *et al*., 1996; MOSS, 2012). Threatens originating from human interventions, as nutrient enrichment and other types of pollution, modifications due to land-use and climate change effects, lead to degradation of inland waters quality resulting in several environmental, sanitary and economic consequences (BRÖNMARK and HANSSON, 2002; CARPENTER *et al*., 2011). To support the assessment of water quality, as well as to assist its improvement, frequent, long-term sustained and spatially distributed data collection and monitoring are required (DÖRNHÖFER and OPPELT, 2016).

Hydroelectric reservoirs are, in special, aquatic systems of notable economic relevance, which also supports the importance of its monitoring. Among the many modifications that occur in these dammed environments, drainage alterations that increase water residence time can be highlighted (TUNDISI and MATSUMURA-TUNDISI, 2008). Greater nutrient availability – related to pollution sources – associated with drainage changes, facilitates excessive phytoplankton proliferation, what makes many reservoirs to become eutrophic environments (TUNDISI, 2008).

Combining the great potential of remote sensing for monitoring water systems, with the significant amount of aquatic color radiometry sensors recently launched and with expanding policies for open data access, remotely sensed data are becoming an even more accessible and cost-effective approach for water quality assessment in inland waters (ZHENG and DIGIACOMO, 2017a).

Among the variety of parameters used for evaluating inland water quality, phytoplankton biomass is a fundamental one, which is used for addressing the trophic status of a water system (ZHENG and DIGIACOMO, 2017b). Phytoplankton biomass is frequently estimated via chlorophyll-*a* (Chl-*a*) concentrations measurements, since it is a photosynthetic pigment that occurs in all phytoplankton species. Through remotely sensed data it is possible to retrieve Chl-*a* and other optically significant constituents (OSCs) concentrations in a aquatic system. Empirical and semi-analytical approaches are common for water constituent retrieval (MOREL, 1980; CARDER *et al*., 1999) and have been extensively investigated and developed (MATTHEWS, 2011; ODERMATT *et al*., 2012). Empirical algorithms directly

relate remote sensed measurements to the constituent of interest, usually through statistical regression, while semi-analytical models are based on radiative transfer inverse modeling.

In this context, Lee *et al*. (2002) developed a quasi-analytical algorithm (QAA) that obtain from remote sensing reflectance (R_{rs}), the inherent optical properties (IOPs) of a water body by combining empirical, semi-analytical and analytical steps. QAA outputs are the backscattering coefficient of suspended particles (b_{bp}) and total absorption coefficient (a_t), and in sequence, from a_t, the absorption coefficient of phytoplankton (a_ϕ) and of colored dissolved organic matter (CDOM) plus detritus (a_{CDM}) are derived. It was originally developed for ocean waters and has been updated since then – currently in its sixth version (LEE, 2014). Due to the direct relationship between OSCs and IOPs, it is possible to obtain Chl-*a* concentrations in a water body from models based on its IOPs.

As reported by Odermatt *et al*. (2012), Chl-*a* retrieval algorithms are commonly presented as band arithmetic based on the Chl-*a* absorption maximums at 442 nm and at 665 nm (BRICAUD *et al*., 1995), reflectance peak at ~700 nm (GITELSON, 1992) and fluorescence emission region at 681 nm (GOWER *et al*., 1999). Therefore, the main configurations of these algorithms, besides the empirical ones, are blue-green – common for ocean waters – (GORDON and MOREL, 1983) and red-near infrared (NIR) – widely used for turbid waters – (GITELSON, 1992; GONS, 1999) band ratio using two, three or four spectral bands. As other water constituents, as CDOM and detritus, present significant absorption in these spectral regions, blue-green band algorithms are not suitable for inland waters, especially because these OSCs do not covary with Chl-*a* in these environments (SUN *et al*., 2012).

Besides presenting OSCs independently variable, inland waters usually presents phytoplankton biomass, CDOM and detritus in higher concentrations than the ones found in open ocean and thus, are considered optically complex systems (PALMER *et al.*, 2015). In addition, OSCs concentrations are significantly variable in different inland water bodies. In this sense, the potential of QAA for addressing IOPs variability is noticeable, as through re-parameterization and calibration of some steps it is also able to retrieve IOPs in different inland water bodies (LE *et al.*, 2009a; YANG *et al*., 2013; MISHRA *et al*., 2013, 2014; LI *et al*., 2013, 2015; WATANABE *et al*., 2016; RODRIGUES, 2017). The complex constitution of inland aquatic systems, in addition to the variation of its optical properties in different water bodies and even within the same one (PALMER *et al*., 2015), explains why bio-optical modeling for these systems is a pertinent investigation subject.

QAA versions re-parameterized for inland waters comprise aquatic environments with different bio-optical properties and most of them are only proved to be suitable for a unique water body. Overall, turbid and eutrophic waters were mostly considered in these investigations. For these environments, main alterations proposed include, fundamentally, shifting the reference wavelength (λ_0) and calibration of empirical steps (YANG *et al*., 2013). The alteration of λ_0 toward longer wavelengths (λ), where pure water absorption is dominant, aims to avoid the influence of OSCs in estimating a_t (LEE *et al.*, 2002; 2009); adjustment of empirical steps of the algorithm intend to adequate to the IOPs of each water environment.

Specifically regarding reservoirs in tropical regions, the first QAA re-parameterized version was developed based on Funil and Itumbiara reservoirs and it is referred as QAA_{CDOM} (OGASHAWARA *et al.*, 2016). This version aimed to be suitable to water systems with greater proportion of CDOM in its OSCs, since further developed versions, to date, were aimed at phytoplankton dominated waters. Watanabe *et al.* (2016) and Rodrigues (2017) versions were configured based on two different reservoirs located in Tietê River cascading system, which is formed by six cascading reservoirs, all built for hydroelectric generation purposes.

For Barra Bonita reservoir (BBHR), the first of them, Watanabe *et al*. (2016) developed QAA_{BBHR} version. The re-parameterization conducted by Rodrigues (2017) was designed for Nova Avanhandava reservoir (NHR), the fifth reservoir of the system, and was named $QAA_{OMW.}$ The most recent QAA original versions – QAA_{V5} (LEE *et al*., 2009) and QAA_{V6} (LEE, 2014) – showed to be unsuitable for both cited reservoirs, presenting errors in magnitudes which make the algorithm, in this form, improper. Ibitinga reservoir (IHR) is also part of the Tietê River cascading system, and it is located downstream from BBHR e upstream from NHR.

The distinct influences arising from the drainage basin (SMITH *et al*., 2014), as well as the variations caused by cascading effect (BARBOSA *et al*., 1999), make the reservoirs along Tietê River to have different compositions. Ecological processes in a cascading reservoir system and, consequently, its water quality parameters, are subject to changes that are considered continuous, as stated by Barbosa *et al*. (1999) through the Cascading Reservoir Continuum Concept (CRCC). The main changes observed by these authors in the Tietê River cascading system were the continuous decrease of turbidity along the system – especially the inorganic fraction – and reduction of nutrients concentration downstream; phytoplankton biomass presented significant decrease only in the latest reservoirs. The hydrodynamic along these systems are also changeable according to the different influences of tributary rivers and

by floodgates opening and closing mechanisms (SMITH *et al.*, 2014). These water systems are also subject to several impacts originating from, as examples, the lack of riparian forest and abundant pollution sources (SMITH *et al.*, 2014). All these processes contribute to the differences in the reservoirs constitutions and, therefore, to the variability in their bio-optical properties.

BBHR and NHR are clear examples of this variability. On one hand, BBHR is classified as a turbid and highly productive aquatic environment, (DELLAMANO-OLIVEIRA *et al.*, 2007), presenting a wide range of Chl-*a* concentrations and organic matter predominance in its SPM (WATANABE *et al*., 2016); this reservoir receives huge pollutant discharges from point and diffuse sources. In contrast, NHR presents, according to seasonal and geographic variations, oligo-to-mesotrophic waters, with low nutrients concentrations and higher proportion of inorganic matter in its SPM (RODRIGUES, 2017).

In IHR, in turn, it has already been observed organic fraction predominance in its SPM and broad spatial and temporal variability of Chl-*a* concentrations (CAIRO *et al*., 2017). According to Novo *et al.* (2013), the trophic state of the reservoir fluctuates from mesotrophic to hypereutrophic, what reinforces the spatial variability characteristic reported by Cairo *et al*. (2017). OSCs ranges observed by Cairo *et al*. (2016) in IHR are intermediaries when comparing with the intervals found in BBHR by Watanabe *et al*. (2016) and in NHR, by Rodrigues (2017). However, some particularities, such as organic predominance in the SPM and higher Chl-*a* concentrations, make IHR characteristics comparable to BBHR ones.

1.2. Hypothesis

Considering that the bio-optical characteristics in IHR are possibly similar to those observed in BBHR, the hypothesis proposed is that, among the assessed algorithms, only QAA_{BBHR} will be able to retrieve accurate values of absorption coefficients of phytoplankton (a_ϕ) for this reservoir and, thus, it will be possible to accurately retrieve Chl-*a* concentrations in IHR from these coefficients. It is still hypothesized that the same QAA version will not be capable of retrieving CDOM plus detritus absorption coefficient (a_{CDM}), since it was re-parameterized considering a phytoplankton dominated water system.

1.3. Objectives

The main objective of this study is to estimate Chl-*a* concentrations in Ibitinga Reservoir via semi-analytical schemes.

1.3.1. Specific objectives

In order to support this central aim, specific objectives are:

(a) To characterize Ibitinga reservoir bio-optically and bio-geochemically;

(b) To assess QAA_{V5}, QAA_{V6}, QAA_{BBHR} e QAA_{OMW} performances for estimating absorption coefficients in the study area and to assess Chl-*a* concentration estimate models for the reservoir;

(c) To analyze Chl-*a* concentrations spatial distribution in the IHR via Ocean and Land Colour Instrument (OLCI) – Sentinel-3A (S3) image, as well as to verify the potential of this sensor for inland water monitoring;

1.4. Dissertation Structure

The dissertation was organized in four chapters. This first chapter (Chapter 1) presents the contextualization of the theme addressed in this research, as well as the hypothesis tested and the objectives proposed. Chapter 2 presents the characterization of the study area and the main information about the field campaigns carried out. Chapters 3 and 4 are structured as scientific papers, composed by introduction of the specific theme, methods – including data acquisition and processing – results, discussions and conclusion. Last chapter (Chapter 5) shows the conclusions about the present study and the recommendations for future work.

The two next paragraphs in this subsection briefly describe what is comprised in Chapters 3 and 4, which correspond to scientific papers already submitted for publication.

CHAPTER 3: POTENTIALS AND LIMITATIONS OF A QUASI-ANALYTICAL ALGORITHM FOR RETRIEVING THE WATER ABSORPTION PROPERTIES IN A CASCADING RESERVOIR SYSTEM

As a first step in the direction of addressing the hypothesis proposed, the first scientific paper was aimed at assessing the suitability of QAA existing versions in retrieving absorption coefficients in the study area. This was the first step in order to verify the possibility of obtaining Chl-*a* concentrations in IHR – which was the final objective – since the following step was dependent of accurate retrieval of the IOPs. Chapter 3 presents the results of the assessment of QAA_{V5}, QAA_{V6}, QAA_{BBHR} and QAA_{OMW} performances in the study area, in terms of a_ϕ and a_{CDM}. The data used was obtained in a dedicated field campaign with 29 sampling stations. Chapter 3 also addresses the bio-optical characterization of IHR.

CHAPTER 4: QUASI-ANALYTICAL ALGORITHM BASED SCHEMES FOR CHLOROPHYLL-A RETRIEVAL IN A TROPICAL RESERVOIR VIA OLCI – SENTINEL-3A IMAGE

Chapter 4 was aimed at assessing schemes for Chl-*a* retrieval in IHR; these schemes are formed by QAA plus models that use absorption coefficients as inputs for obtaining Chl-*a* concentrations. In this chapter, an OLCI – S3 image was used for analyzing the spatial distribution of Chl-*a* in the study area. The four absorption coefficients based models tested were calibrated for IHR using *in situ* data from the first fieldwork, and cross-validated; each one of the four models were calibrated using absorption coefficients originated from QAA_{V5}, QAA_{V6}, QAA_{BBHR} and $QAA_{OMW,}$ resulting in sixteen models. After that, all the schemes (QAA plus model calibrated from its outputs) were applied to the OLCI image atmospherically corrected, since all of them presented reasonable accuracy after validation. The performances of the sixteen schemes in obtaining Chl-*a* concentrations in IHR were assessed through new *in situ* data from a second fieldwork, coincident with the image acquisition date.

CHAPTER 2: STUDY AREA

2.1. Characterization

Ibitinga reservoir was built for hydroelectric generation purpose and operates as a run-of-river system. It lies in a transitional region between tropical and subtropical climate, specifically in a humid subtropical climate, characterized by well-defined dry and wet seasons. IHR is located in the middle course of Tietê River, central area of São Paulo State, Brazil (21º45' S and 48º 59' W). It is the third of six cascading reservoirs, with Barra Bonita and Bariri reservoirs located upstream and Promissão, Nova Avanhandava and Três Irmãos reservoirs downstream (Figure 1 (b)). Its flooded area is around 114 km², with approximately 9 m of average depth and an average flow of 525 $m^3 s^{-1}$. The two main tributary rivers are Jacaré-Guaçu and Jacaré-Pepira, and the reservoir extends over 70 km in Tietê River plus 25 km over each one of its main tributaries (LONDE *et al*., 2016).

The surrounding area presents grazing land, sugarcane crops and minor areas of reforestation and secondary vegetation (GUIMARÃES *et al*., 1998). The river receives wastewater discharges from domestic and industrial sources along its course, in special huge amounts originating from São Paulo city, located upstream of the reservoir. The catchment area also comprises diffuse sources of pollution, as agriculture – notably sugarcane crops – and cattle breeding activities; IHR is inserted in a region that presented significant expansion of sugarcane cultivation in the past ten years (RUDORFF *et al*., 2010). The trophic state of the reservoir is highly spatially and temporally variable, comprising mesotrophic to eutrophic regions (NOVO *et al*., 2013; CAIRO *et al*., 2017). Londe *et al.* (2016) show, via remote sensing, how the changes in water residence time over the hydrological year affect the phytoplankton proliferation and its spatial distribution in IHR, reaffirming the evidences of fluctuation in its trophic state. The authors found a link between increasing of water residence time and water surface coverage by phytoplankton blooms.

The Water Resources Management Unit in which IHR is inserted (UGRHI 13, Tietê-Jacaré) supplies water resources for multiple uses, as domestic and industrial supply, irrigation, navigation, domestic and industrial wastewater discharge, as well as hydroelectric energy generation (CETESB, 2005). This management unit has presenting increasing demand for urban uses and the availability of water *per capita* presents a reduction trend over the years, what can be associated to population growth (CBH – TJ, 2013). Also, Tietê-Jacaré

watershed has one of the lowest rates of natural vegetation remaining in São Paulo State, presenting only 2.2% of the vegetation cover in the State.

2.2. Field Campaigns

Two field campaigns, hereafter referred to as IBI1 and IBI2, were conducted respectively between July 19 and 23, 2016 and on June 21, 2017 – austral winter – in order to obtain water quality data, spectral data and water samples in 29 sampling stations in IBI1 and 6 stations in IBI2 (Figure 1 (c)). IBI1 data were already described by Andrade *et al*. (2017, submitted).

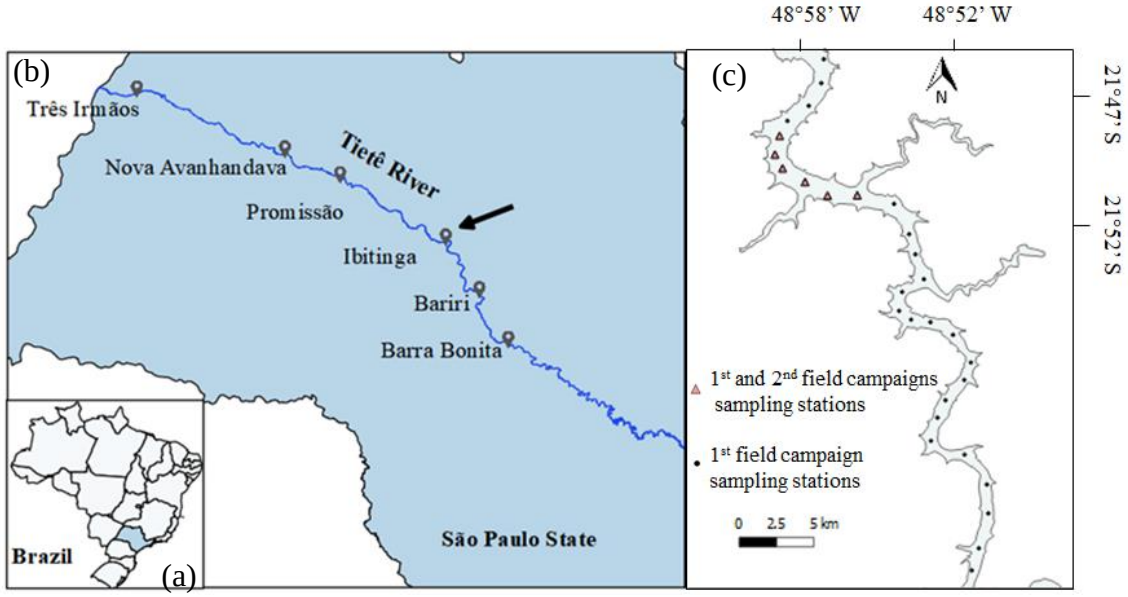

Figure 1. (a) São Paulo State location in Brazil; (b) Cascading reservoirs in Tietê River. Please note Ibitinga Hydroelectric Reservoir (black arrow) upstream from Nova Avanhandava reservoir and downstream from Barra Bonita reservoir (see text for more details); (c) Distribution of sampling stations from IBI1 (July, 2016) and IBI2 (June, 2017) field campaigns in the study area.

Figure 2 presents the average of daily precipitation rate (millimeters per day) in the reservoir and surrounding area, from June, 2016 to June, 2017. It can be observed that the first field (July, 2016) campaign occurred after a significant period of reduced precipitation, what was expected since it happened during the dry season in the region. However, the second period of data collection (June, 2017), despite of also performed in the dry season, was preceded by days of intense rainfall.

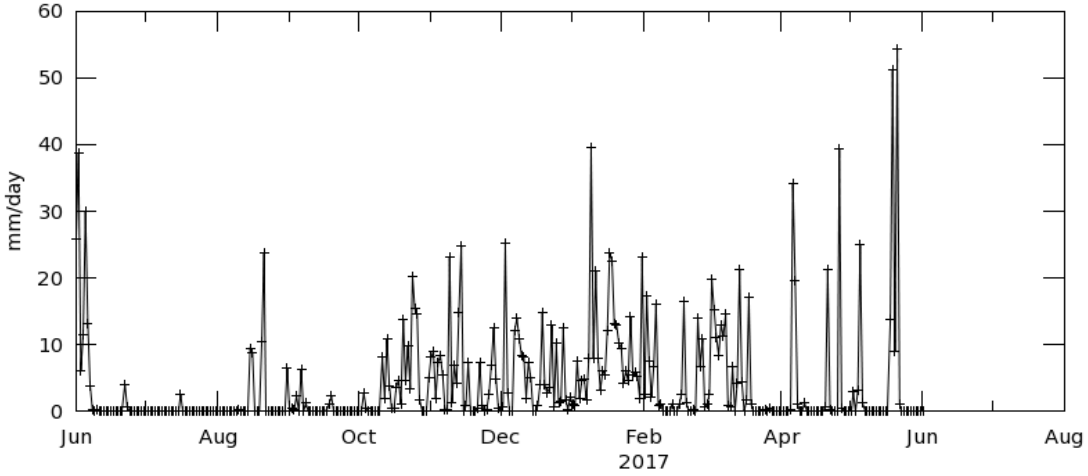

Figure 2. Area-averaged of precipitation rate from June, 2016 to June, 2017. Source: NASA/GIOVANNI (https://giovanni.gsfc.nasa.gov/giovanni/).

CHAPTER 3: POTENTIALS AND LIMITATIONS OF A QUASI-ANALYTICAL ALGORITHM FOR RETRIEVING THE WATER ABSORPTION PROPERTIES IN A CASCADING RESERVOIR SYSTEM

3.1. Introduction

The applicability of Quasi-Analytical Algorithm (QAA) (LEE *et al.*, 2002) in optically complex inland waters is certainly more challenging than when working on Case 1 waters (ODERMATT *et al*., 2012). In order to make QAA suitable for more complex waters, calibration and re-parameterization of the original versions are required, as demonstrated by several authors (see for example, LE *et al*., 2009a; YANG *et al*., 2013; MISHRA *et al*., 2013, 2014). When it comes to cascading reservoirs systems, variability trends are also influenced by cascading effects (BARBOSA *et al*., 1999), as well as by the different contributions arising from the drainage basin, tributary rivers and floodgates mechanisms (SMITH *et al*. 2014). In such aquatic systems there are widely differing optical properties and the efficiency of parameterized versions is uncertain.

Tietê River cascading system is located in São Paulo state, a densely populated region of Brazil where water quality is an urgent matter. Recently, two QAA versions were parameterized for two reservoirs from this system: QAA_{BBHR} (WATANABE *et al*., 2016) and QAA_{OMW} (RODRIGUES, 2017). The QAA_{BBHR} was parameterized for the eutrophic Barra Bonita Hydroelectric Reservoir (BBHR) (DELLAMANO-OLIVEIRA *et al*., 2008), which is the first reservoir of the cascading system, receiving large amounts of pollutants from the metropolis of São Paulo and also from agriculture and cattle raising (BARBOSA *et al.*, 1999). Suspended particulate matter (SPM) in this reservoir is dominated by the organic fraction (SMITH *et al*., 2014; WATANABE *et al*., 2016). The QAA_{OMW} version was parameterized for the oligo-to-mesotrophic Nova Avanhandava Reservoir (NHR), located further downstream, presenting relatively lower Chlorophyll-*a* (Chl-*a*) and SPM concentrations, and inorganic predominance in its SPM (SMITH *et al*., 2014).

Ibitinga Hydroelectric Reservoir (IHR) is also situated in the Tietê River, downstream from BBHR and upstream from NHR. Chl-*a* and SPM concentrations values in IHR are typically within the ranges found in BBHR and NHR (CAIRO *et al*., 2017). However, due to some particularities, as organic matter predominance and slightly higher Chl-*a* concentrations, IHR is possibly more similar to BBHR bio-optical characteristics. Considering that IHR bio-optical status is comparable to BBHR one, the hypothesis here tested is that QAA_{BBHR} could be able to consistently retrieve absorption coefficients of phytoplankton pigments (a_ϕ) in IHR,

but may be not capable of accurately retrieve the colored dissolved organic matter (CDOM) plus detritus (a_{CDM}) absorption coefficient, as QAA_{BBHR} was parameterized considering phytoplankton features of the BBHR reservoir (WATANABE *et al*., 2016).

To test the aforementioned hypothesis we aim to assess the performance of QAA_{BBHR} and QAA_{OMW}, besides two latest native forms of QAA - QAA_{V5} and QAA_{V6} (LEE *et al.*, 2009 and LEE, 2014, respectively) - in retrieving a_ϕ and a_{CDM} for IHR. We decided to also test the QAA_{V5} and v_6 in order to compare the results from the original and re-parameterized versions. This investigation relates to the purpose of monitoring all cascading system in an integrated manner, through a unique QAA version properly adjusted for capturing the bio-optical variability occurring along the system. We also addressed water quality and bio-optical characterization of IHR, intending to associate it with algorithms efficiency, as this was not previously reported in the literature.

3.2. Material and Methods

3.2.1. Water quality data

Secchi disk depth (m), turbidity (NTU) and electric conductivity (µs/cm) data were obtained in all 29 sampling stations (Figure 1(c)). Water samples were collected in order to estimate Chl-*a* concentration, through acetone extraction method (GOLTERMAN *et al.*, 1978; LORENZEN *et al.*, 1967). The SPM concentrations, as well as organic (OSM) and inorganic suspended matter (ISM) fractions were estimated according to the American Public Health Association protocol (APHA, 1998).

3.2.2. Radiometric Data

Total upwelling radiance ($L_t(\lambda)$; W m^{-2} sr^{-1} nm^{-1}) and atmospheric diffuse radiance ($L_s(\lambda)$; W m^{-2} sr^{-1} nm^{-1}) were measured using two RAMSES-ARC hyperspectral radiometers. Downwelling irradiance ($E_d(\lambda)$; W m^{-2} nm^{-1}) was measured using a RAMSES-ACC sensor (TriOS, Oldenburg, Germany). All radiometric sensors used operate in the spectral range between 350 and 900 nm, with a spectral resolution of 3.3 nm. The acquisition geometry followed Mobley (1999), with $L_t(\lambda)$ measured at a zenith angle (θ) of 140°, $L_s(\lambda)$ at θ=40° and $E_d(\lambda)$ measured with the sensor aligned to the zenith, i.e., θ=0°; all measurements were taken at an azimuth angle of 90° (Figure 3).

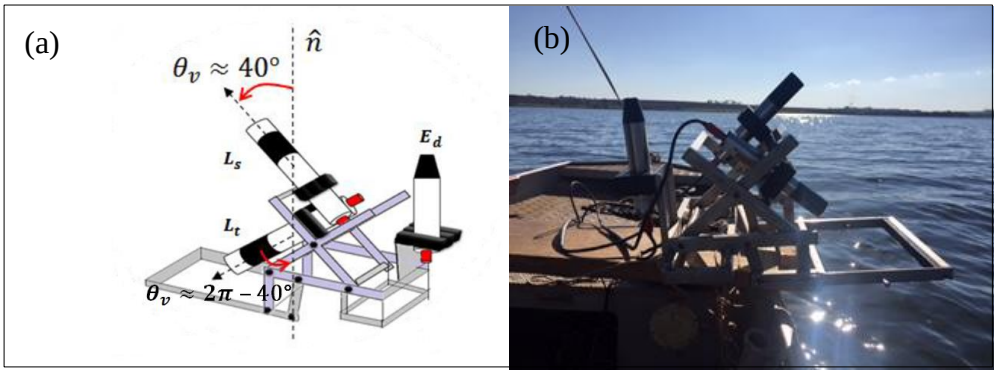

Figure 3. (a) Acquisition geometry proposed by Mobley (1999). Adapted from Rodrigues (2017); (b) Radiometric sensors arrangement in field works.

These radiometric quantities were then applied to estimate remote sensing reflectance ($R_{rs,}$ sr^{-1}) spectra, using the spectral optimization approach proposed by Lee *et al.* (1999), in order to remove surface-reflected radiance ($L_r(\lambda)$) (LEE *et al.*, 2010). R_{rs} spectra, which were estimated through *in situ* hyperspectral measurements, were then resampled to simulate

satellite data. The spectral response functions of each Ocean and Land Colour Instrument (OLCI) – Sentinel-3A bands were used to derive band-weighted data.

3.2.3. Phytoplankton absorption coefficient (a_ϕ) and Detritus plus CDOM absorption coefficient (a_{CDM})

To estimate CDOM absorption coefficient (a_{CDOM}, m^{-1}), water samples previously filtered through GF/F Whatman fiberglass filters – 0.7 μm porosity – were again filtered through Whatman nylon membrane – 0.22 μm porosity and 47 mm diameter. The absorbance of the filtrates was read using a 2600 UV-VIS spectrophotometer (Shimadzu, Japan), and the results were applied to calculate a_{CDOM} as proposed by Bricaud *et al*. (1981) (Eq.1).

$$a_{CDOM} = 2.3\frac{OD_{CDOM}(\lambda)}{r} \qquad \text{(Eq.1)}$$

where $OD_{CDOM}(\lambda)$ is the optical density of CDOM and r is the cuvette path length (0,1m).

To determine the total particulate (algal and detritus) absorption coefficient (a_p, m^{-1}), water samples were filtered through fiberglass GF/F Whatman – 0.7 μm porosity and 47 mm diameter. Then, Transmittance-Reflectance (T-R) method described by Tassan and Ferrari (1995, 1998) was employed using a double-beam 2600 UV-VIS spectrophotometer equipped with an integrating sphere. The spectral sampling ranged from 280 nm to 800 nm, with a spectral resolution of 1 nm. In order to bleach pigments from the filters, a 10% sodium hypochlorite (NaCLO) solution was used and T-R measurements were taken again. By eliminating pigments influence, it was possible to obtain detritus absorption coefficient (a_d, m^{-1}); a_p and a_d are then obtained according to Eq.2:

$$a_{p,d}(\lambda) = \frac{2.303\ OD_{p,d}(\lambda)}{V.A} \qquad \text{(Eq. 2)}$$

where $OD_p(\lambda)$ is the optical density of total particulate, $OD_d(\lambda)$ is the optical density of detritus, V is the filtered volume (m^3) and A is the filter clearance area (m^2). The phytoplankton absorption coefficients (a_ϕ, m^{-1}) were calculated by subtracting a_d from a_p. Finally, a_{CDM} is calculated by adding a_{CDOM} to a_d.

3.2.4. QAA

QAA_{V5} and QAA_{V6} performances were evaluated for IHR. It is important to highlight that QAA_{V6} was developed in order to improve QAA accuracy in water systems in which R_{rs}

at 670 nm is greater than 0.0015 sr^{-1}, i.e., coastal regions and areas with high sediments concentration. QAA_{BBHR} and QAA_{OMW}, the two re-parameterized versions for Tietê River cascading system were also tested. The dataset considered by Watanabe *et al.* (2016) for QAA_{BBHR} parameterization presented high values and a broad range of Chl-*a* concentration (from 17.7 to 797.8 mg m^{-3}; average 274.5 mg m^{-3}) and SPM concentration ranging from 3.6 to 44.0 g m^{-3} (average 14.6 g m^{-3}) , with its organic fraction corresponding to approximately 90% of total SPM in the samples. Differently, the dataset used by Rodrigues (2017) for QAA_{OMW} parameterization showed low average Chl-*a* concentration (16.15 mg m^{-3}, ranging from 2.46 to 38.59 mg m^{-3}), as well as low average SPM concentration (1.85 g m^{-3}, varying from 0.10 to 5.30 g m^{-3}); inorganic fraction was predominant in total SPM. Statistic metrics used to assess the QAAs performances for IHR were normalized root mean square error (nRMSE) and mean absolute percentage error (MAPE), considering a_ϕ and a_{CDM} estimated from water samples obtained in the field campaign as reference data.

3.3. Results and Discussion

3.3.1. Water quality characterization

Chl-*a* and SPM concentrations varied widely (1.37 - 119.04 mg m^{-3} and 1.00 - 8.10 g m^{-3}, respectively), showing significant spatial variability (Table 1). OSM represented 63% of the SPM, which means organic matter is slightly predominant. Turbidity values also showed some fluctuation, although it was lower than the variation presented by Chl-*a* and SPM (coefficient of variation 23.28%); in general, turbidity presented a relative low average value (4.24 NTU). Secchi disk presented an average of 2.23 m and the lowest coefficient of variation (15.50%).

Table 1. Descriptive statistics of water quality parameters in IHR; SD: standard deviation; CV: coefficient of variation; n = 29.

	Minimum	**Maximum**	**Mean**	**SD**	**CV (%)**
Chl-*a* (mg m^{-3})	1.37	119.04	19.34	24.71	127.79
SPM (g m^{-3})	1.00	8.10	2.45	1.40	57.19
OSM/SPM	0.29	0.88	0.63	0.15	23.28
ISM/SPM	0.12	0.71	0.37	0.15	40.11
Depth (m)	9.50	21.60	14.90	4.29	28.77
Turbidity (NTU)	2.82	8.87	4.24	1.19	28.01
Secchi Depth (m)	1.60	3.20	2.23	0.35	15.50
$a_\phi(443)$ (m^{-1})	0.06	1.88	0.30	0.36	120.44
$a_{CDM}(443)$ (m^{-1})	1.24	5.93	1.95	0.83	42.41
$a_d(443)$ (m^{-1})	0.14	0.62	0.37	0.13	33.54
$a_{CDOM}(443)$ (m^{-1})	0.87	5.31	1.57	0.80	50.85

Regarding the absorption coefficients, a_d (443) and a_ϕ (443) presented similar average values, while $a_{CDOM}(443)$ presented the highest values - greater than a_d (443) and a_ϕ (443). Detritus can be constituted of mineral matter, humus or organic remains; considering that organic fraction of SPM showed to be slightly higher in this dataset and a_ϕ is not dominant, detritus in the reservoir is probably mainly constituted of humus and organic remains that are not resulting from phytoplankton degradation.

3.3.2. Bio-Optical Characterization

In situ measured R_{rs} spectra (Figure 4 (a)) shows absorption features around 675 nm and a reflectance peak around 700 nm that can be associated with Chl-*a*. However, these R_{rs} features are not observed in all stations, indicating spatial variability in terms of optically significant constituents (OSC) at IHR. A prominent feature of reflectance in the green spectral region, around 550 nm, can be observed with different magnitudes (Figure 4 (a)). This reflectance peak is usually related with scattering from algal cells (GITELSON, 1992), and also with inorganic suspended matter, which shifts higher reflectance values toward longer wavelengths (HAN and RUNDQUIST, 1997). Average a_{CDOM} was the greater contributor for a_t until around 660 nm (Figure 4 (b)). Average a_d presented higher values than average a_ϕ through blue and green spectral regions; approximately at 600 nm average a_ϕ shows slight increase, and it is considerably greater than average a_d from 660 nm to 700 nm (Figure 4 (b)).

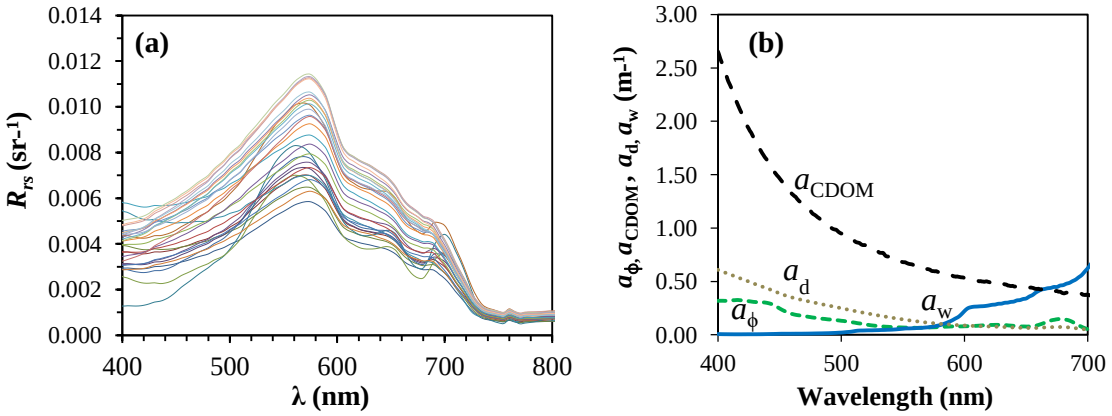

Figure 4. (a) *In situ* R_{rs} spectra; (b) Average absorption coefficients by phytoplankton (a_ϕ), CDOM (a_{CDOM}), detritus (a_d) and pure water (a_w); n=29.

Ternary plots (Figure 5) display the relative contribution of a_{CDOM}, a_ϕ and a_d to the total absorption at IHR. Similar datasets from BBHR (WATANABE *et al.*, 2016) and NHR (RODRIGUES, 2017), collected in May, 2014 and May, 2016, respectively are also plotted for comparison purpose. It is relevant to highlight that all three dataset considered here were collected during the dry season.

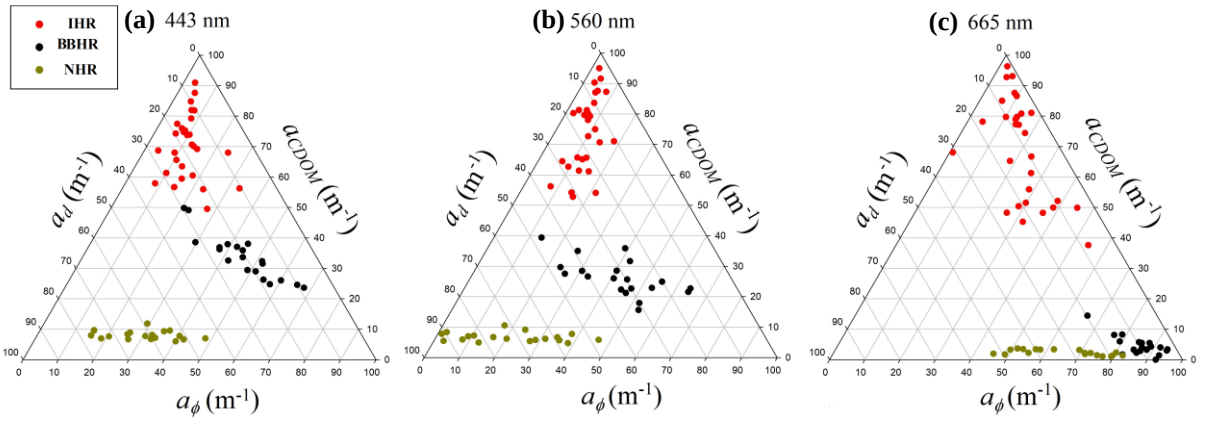

Figure 5. Ternary plots presenting the relative contribution of detritus, phytoplankton and CDOM to the total absorption (without water fraction) at three different wavelengths for IHR (red dots), BBHR (black dots) and NHR (brown dots): (a) 443 nm; (b) 560 nm; (c) 665 nm.

Absorption in IHR dataset is dominated by CDOM in all three wavelengths here considered, corresponding to 70.11 ± 3.94% at 443 nm, 73.63 ± 4.67% at 560 nm and 68.94 ± 6.43% at 665 nm. Detritus contributed to the total absorption budget with 18.13 ± 2.67% at 443 nm and 17.18 ± 3.40% at 560 nm. At 665 nm, phytoplankton contributed with 20.08 ± 5.27% of the total while detritus contributed with only 10.97 ± 2.86%. In BBHR, total absorption was predominately due to phytoplankton in all three wavelengths, especially at 665 nm, with a_ϕ contributing with 85.72±3.18%. However, at 443 nm and 560 nm the total absorption is more balanced among all OSC, as can be observed in the scatter of dots around the central area of the plots (Figures 5 (a) and 5 (b)).

In NHR dataset, otherwise, a_d was the major contributor at 443 nm and 560 nm, corresponding to 62.16±4.42% and 72.02±6.52%, respectively. At 665 nm a_ϕ represented 65.15±5.97% of total absorption, while a_d was the second greater contributor with 32.51±5.72%. These differences may be related to factors as the cascading effect (BARBOSA *et al.*, 1999); this concept explains the changes in the water quality parameters occurring along a cascading system as reduction of turbidity, nutrients concentration and phytoplankton biomass in Tietê River downstream reservoirs. It also can be related to the changeable allochthonous contributions arriving in each reservoir.

3.3.3. QAA performances

QAA_{OMW} presented the lowest average nRMSE (%) and MAPE (m^{-1}) for a_ϕ retrieval (Table 2). However, if we consider only 665 nm band, which is a diagnosis wavelength for

Chl-*a*, this same version shows the highest errors (nRMSE = 31.74%, MAPE = 6.03 m^{-1}). QAA_{OMW} tuning was based on NHR dataset, comprising Chl-*a* concentration values lower than the ones measured in IHR (NHR average 7.94 mg m^{-3}; IHR average 19.34 mg m^{-3}), and this difference can be related to its poor performance at 665 nm band (RODRIGUES, 2017). QAA_{BBHR}, differently, was developed for a highly productive reservoir, and IHR bio-optical status did not show to be similar to BBHR one, justifying why it was not completely suitable for retrieving IOPs in IHR. QAA_{V6} showed higher values of nRMSE and MAPE than QAA_{V5} in all wavelengths, although this performance was not initially expected since QAA_{V6} was proposed for R_{rs} (670) > 0.0015 sr^{-1}, which fits IHR dataset (R_{rs} (670) = 0.00427 sr^{-1}). Comparatively, QAA_{V5} showed to be the most accurate version at 665 nm (NMRSE = 15.35%, MAPE = 1.19 m^{-1}).

Table 2. QAAs performances for a_ϕ retrieval, according to each band, based on nRMSE (%) and MAPE (m^{-1}).

	QAA_{V5}		**QAA_{V6}**		**QAA_{BBHR}**		**QAA_{OMW}**	
Bands (nm)	nRMSE %	MAPE (m^{-1})	nRMSE %	MAPE (m^{-1})	nRMSE %	MAPE (m^{-1})	nRMSE %	MAPE (m^{-1})
412	14.04	1.36	17.14	1.93	19.46	0.70	21.94	1.84
443	15.86	1.35	19.82	1.91	13.80	0.86	21.02	1.15
490	30.77	2.44	40.53	3.29	30.86	2.46	26.07	0.98
510	32.46	2.61	44.12	3.58	35.94	2.86	19.92	0.67
560	38.14	3.21	54.41	4.55	49.70	4.03	20.49	0.60
620	14.19	1.38	21.25	3.49	20.01	3.48	16.07	0.84
665	15.35	1.19	20.23	4.09	18.06	5.46	31.74	6.03
681	15.49	0.78	19.17	2.32	14.03	2.56	23.79	1.94
709	112.00	3.78	118.04	10.99	89.48	10.70	30.64	0.45
Average	**32.03**	**2.01**	**39.41**	**4.02**	**32.37**	**3.68**	**23.52**	**1.61**

Scatterplots of a_ϕ estimated by the QAAs and a_ϕ measured in laboratory are shown in Figure 6. In general, QAA_{V5} overestimated a_ϕ in great part of wavelengths (Figure 6 (a)), except for the longer ones – specifically 681 and 709 nm – for which the version underestimated the values. The other versions overestimated most of a_ϕ values at all wavelengths, excluding QAA_{BBHR} at 412 nm. It can be clearly observed that a sampling spot

disagrees with the other ones in almost all wavelengths for all four QAA tested; this spot corresponds to the highest Chl-*a* and SPM concentrations of the dataset.

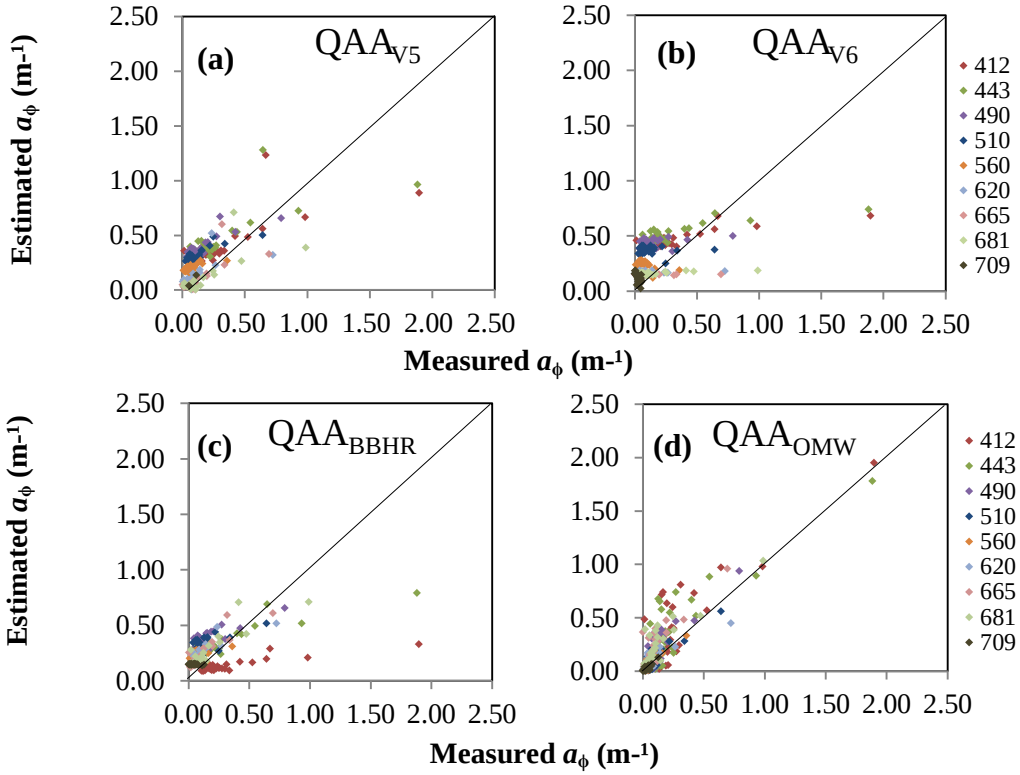

Figure 6. Comparison between estimated and measured a_ϕ using: (a) QAA$_{V5}$; (b) QAA$_{V6}$; (c) QAA$_{BBHR}$; and (d) QAA$_{OMW}$.

For a_{CDM}, all QAAs variants demonstrated similar average nRMSE and MAPE, presenting reasonable accuracy (Table 3). An improvement of nRMSE values can be observed with increasing wavelengths. QAA$_{OMW}$ showed slight better results (nRMSE = 21.74%, MAPE = 0.44 m^{-1}); NHR is a non-productive reservoir and it is dominated by a_{CDM} in the blue-green region, just as IHR, and this can be associated with the lower errors presented by QAA$_{OMW}$.

Table 3. QAAs performances for a_{CDM} retrieval, according to each band, based on nRMSE (%) and MAPE (m^{-1}).

	QAA_{V5}		**QAA_{V6}**		**QAA_{BBHR}**		**QAA_{OMW}**	
Bands (nm)	nRMSE %	MAPE (m^{-1})	nRMSE %	MAPE (m^{-1})	nRMSE %	MAPE (m^{-1})	nRMSE %	MAPE (m^{-1})
412	50.41	0.85	49.60	0.84	41.17	0.67	29.49	0.35
443	40.71	0.87	40.26	0.86	34.54	0.70	24.64	0.31
490	32.75	0.91	32.56	0.90	29.54	0.78	21.43	0.33
510	30.46	0.92	30.33	0.91	28.07	0.81	20.69	0.34
560	25.94	0.95	25.89	0.94	24.83	0.86	19.71	0.39
620	23.52	0.97	23.50	0.97	23.07	0.92	19.82	0.49
665	22.42	0.98	22.41	0.98	22.20	0.95	19.98	0.57
681	21.91	0.98	21.91	0.98	21.74	0.96	19.85	0.58
709	21.65	0.99	21.65	0.99	21.54	0.97	20.07	0.64
Average	**29.97**	**0.94**	**29.79**	**0.93**	**27.41**	**0.85**	**21.74**	**0.44**

Figure 7 shows that QAA_{V5}, QAA_{V6} and QAA_{BBHR} consistently underestimated a_{CDM} in all wavelengths. It probably occurs due to high CDOM and detritus concentrations and its relative predominance in the absorption budget of IHR (see Figure 5) that is not commonly found in ocean and coastal waters, and also differs from BBHR optical characteristics. In these scatterplots, two sampling spots evidently differ from the others: one of them is discrepant in all wavelengths and also corresponds to the spot with the highest Chl-*a* and SPM concentrations, while the second one disagrees mostly in the shortest wavelengths - except for QAA_{OMW}, which overestimated a_{CDM} values for all wavelengths - and it corresponds to the second highest SPM concentration in the dataset.

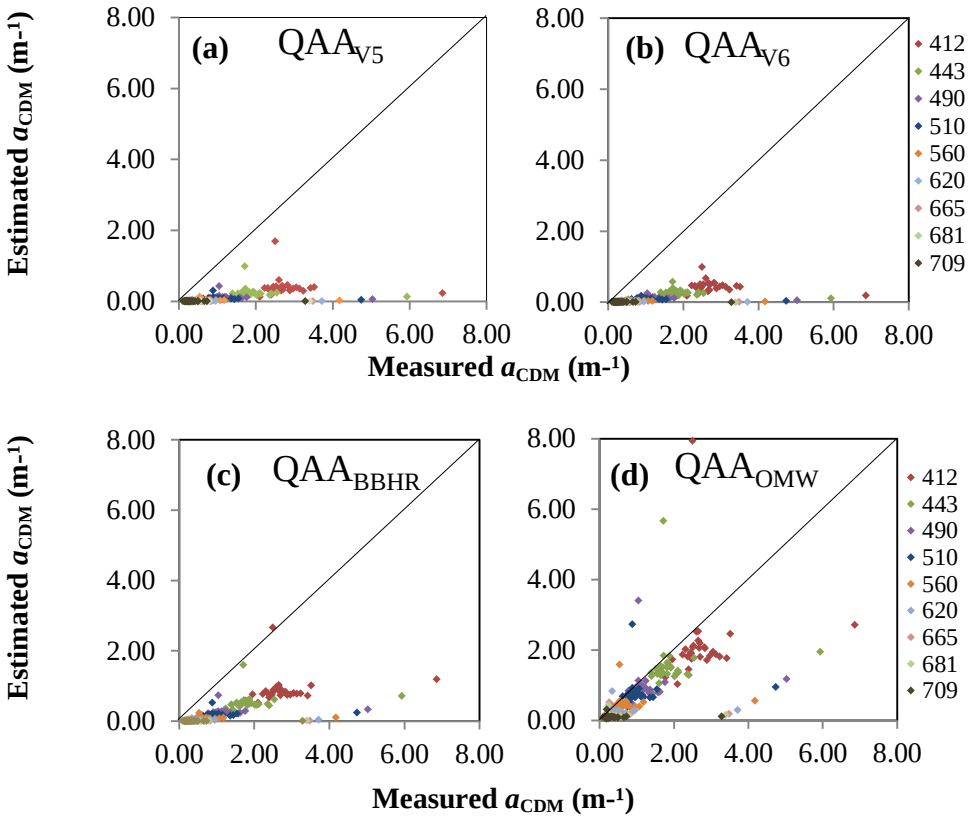

Figure 7. Comparison between estimated and measured a_{CDM} using: (a) QAA$_{V5}$; (b) QAA$_{V6}$; (c) QAA$_{BBHR}$; and (d) QAA$_{OMW}$.

On the other hand, QAA$_{OMW}$ was able to retrieve, in general, more consistent values of a_{CDM} (Figure 7 (d)). It is important here to highlight that QAA approach integrates the absorption by detritus and CDOM as a_{CDM}. Taking this into account, and also considering that NHR absorption occurs mostly due to detritus, while in IHR the CDOM is predominant, it corroborates the capability of QAA$_{OMW}$ in retrieving a_{CDM} in non-phytoplankton dominated waters and, consequently, its potential in determining carbon content in aquatic systems.

3.3.4. Implications for OSC monitoring

Neither originals nor re-parameterized QAA versions here tested were capable of estimating accurately the absorption coefficients in all wavelengths. This shows a challenge in coping with high optical variability in cascading system. Although QAA$_{BBHR}$ was parameterized for a high productive aquatic system, the model could not accurately retrieve the a_ϕ at 665 nm (a_ϕ (665)), which is used as a proxy to estimate Chl-*a* concentration. This could have happened because Chl-*a* concentration values in BBHR are very high (~ 797 mg m^{-3}), and due to the fact that the R_{rs} spectra is masked by the package effect, as reported by Alcântara *et al*. (2016). For a_ϕ (665) the QAA$_{V5}$ presented the lowest error. On the other hand,

to estimate the a_{CDM} at 443 nm (a_{CDM} (443)), which is a proxy for carbon content, the QAA_{OMW} presented the lowest error. These results highlighted the limitation of such quasi-analytical scheme in order to monitor the spatial-temporal OSCs in the cascading system. However, the obtained results also represents an opportunity to better understand the complexity of these aquatic systems and to figure out how to improve the QAA in order to use only one version to estimate the OSCs in the entire cascade. Up to now the monitoring of OSCs from space operationally is still a challenge.

3.4. Conclusion

Since QAA native versions, QAA_{V5} and QAA_{V6}, were designed for ocean and coastal waters, a poor performance for optically complex inland waters was already expected and it was here confirmed. However, QAA_{BBHR} did not perform satisfactorily as supposed, demonstrating that even presenting some similarity regarding the OSCs, the bio-optical status of BBHR and IHR are substantially different and, thus, IHR IOPs cannot be derived through this re-parameterized QAA. Although QAA_{OMW} was able to retrieve relatively accurate average values for a_{CDM} and a_{ϕ} in IHR, it presented an unsuitable performance for a_{ϕ} at 665nm, indicating that this version also has its limitations for deriving IHR IOPs. Therefore, our hypothesis can be rejected, since QAA_{BBHR} was not suitable for retrieving neither a_{ϕ} nor $a_{CDM.}$ Variability of bio-optical characteristics along the cascading system was confirmed, since none re-parameterized version for reservoirs in the same system was completely suitable for IHR. The re-parameterized versions showed not to be sensitive to the variations occurring in the cascade. Further research is necessary, aiming to achieve a QAA re-parameterization appropriate for IHR and, prospectively, for the whole Tietê River cascading system.

Acknowledgements

The authors thank FAPESP Projects (Process N° 2012/19821-1 and 2015/21586-9) and Professor Edivaldo Velini and staffs from FCA/UNESP for allowing the use of their laboratory facilities.

CHAPTER 4: QUASI-ANALYTICAL ALGORITHM BASED SCHEMES FOR CHLOROPHYLL-*A* RETRIEVAL IN A TROPICAL RESERVOIR VIA OLCI – SENTINEL-3A IMAGE

4.1. Introduction

Inland waters are sensitive to anthropogenic disturbances and have been affected by environmental changes resulting from these pressures, what clearly explains the demand for assessing and monitoring water quality parameters (PALMER *et al.*, 2015). Besides the known potential of remote sensing for monitoring lakes, reservoirs and rivers (BUKATA, 2013), it is still challenging to retrieve optical and biogeochemical properties in these commonly optically complex water systems (MOUW *et al*., 2015; PALMER *et al*., 2015). Water optically significant constituents such as phytoplankton pigments, suspended particulate matter (SPM) and colored dissolved organic matter (CDOM), vary widely and independently to each other in inland waters. These constituents, called optically significant constituents (OSC), are directly related to water quality. OSC variation is also substantial between different inland water bodies, increasing the obstacles for the development of a universally applicable model for quantifying their concentrations from remote sensing measurements.

Chlorophyll-*a* (Chl-*a*), in particular, is a photosynthesizing pigment that occurs in all phytoplankton species and, thus, is a key parameter for water quality. Besides its role in carbon sequestration and primary productivity (ROESLER *et al*., 1989), phytoplankton excessive proliferation can lead to eutrophication processes (AYRES *et al*., 1996). Therefore, Chl-*a* concentration is considered the main variable to indicate the trophic state of aquatic environments, serving as a proxy of their ecological health.

While relatively simple blue-to-green band-ratio algorithms presents acceptable results for Chl-*a* retrieval in open ocean (O'REILLY *et al*., 1998), they are inadequate for inland waters, due to a greater influence of other OSC, such as CDOM and detritus, which present strong contribution in the absorption budget at these spectral regions. Aiming to quantify Chl-*a* and other OSC, several algorithms based on remote sensing measurements were developed (ODERMATT *et al*., 2012). These algorithms can be classified in empirical, which relate remote sensing reflectance (R_{rs}) or irradiance reflectance (R) to Chl-*a* through statistical regression, and semi-analytical, based on the radiative transfer theory (MOREL, 1980; CARDER *et al*. 1999). While the first present limitations for widening temporal and spatial application, the second often require input parameters and their performance depend on the

representativeness of the model used for estimating the inherent optical properties (IOPs) of the environment in which it is being applied.

Quasi-analytical algorithm (QAA), a special case which includes empirical and analytical steps for retrieving absorption, *a*, and particle backscattering, b_{bp}, coefficients (LEE *et al*., 2002), represents a great contribution in this sense. It is broadly applicable for ocean waters, for which it was originally parameterized. Re-parameterizations and calibrations can make QAA suitable for inland waters. Nonetheless, until now, each parameterization is only proven to be suitable for a unique water body (LE *et al.*, 2009a; YANG *et al*., 2013; MISHRA *et al*., 2013, 2014; LI *et al*., 2013, 2015; WATANABE *et al*., 2016; RODRIGUES, 2017, among others). These versions were mainly developed for turbid and eutrophic waters. In order to adapt QAA for these waters, the main enhancements proposed by the authors were the shift of reference wavelength to near-infrared bands, adjustment of spectral slope for particle backscattering and calibration of other empirical steps. Changing reference wavelength to longer wavelengths, where pure water absorption is dominant, aims to avoid OSC influences in $a(\lambda)$ estimation (LEE *et al*., 2002); other changes intend to adequate the algorithm to the IOPs of each water system.

Further assessment of how QAAs versions perform in different inland water bodies, goes in the direction of expanding its applicability. By integrating QAA with models that use absorption coefficients – QAA outputs – as inputs, it is possible to compose schemes for Chl-*a* concentration retrieval. Chl-*a* monitoring in a reservoir is addressed in this study, which is aimed at assessing the suitability of schemes composed by QAA plus absorption coefficients based models, in order to obtain Chl-*a* concentration in the Ibitinga Reservoir, Tietê River, Brazil, via Ocean and Land Colour Instrument (OLCI) image. Originals and re-parameterized QAA versions were assessed, as well as four absorption coefficients based models. In order to support this main objective, specific aims were: to carry out optical and biogeochemical characterization of the study area; to analyze spatial distribution of Chl-*a* concentrations in Ibitinga Reservoir; and to assess OLCI image performance for Chl-*a* retrieval in an inland water body. Since the sensor recently became operational – first data released in October, 2016 (ESA, 2016) – its use for inland water monitoring still has great potential to be investigated.

4.2. Methods

4.2.1. Water quality data

Water samples collected just below air-water interface in the sampling stations were used for estimating Chl-*a* and suspended particulate matter (SPM) concentrations. Secchi disk depth (m), turbidity (NTU) and electric conductivity (μs/cm) data were also acquired in all IBI1 and IBI2 stations, using respectively a Secchi disk, a turbidimeter and a conductivity meter.

Chl-*a* concentration is determined via acetone extraction method (GOLTERMAN *et al.*, 1978), through which samples are filtered using Whatman fiberglass filters – 0.7 μm porosity and 47 mm diameter – on the day of collection and frozen until laboratory analysis. In sequence, the filters are macerated with 10 ml of acetone solution (90%) and centrifuged. Absorbances at wavelengths of 665 and 750 nm of the resulting liquid phase are determined by spectrophotometry, before and after acidification with hydrochloric acid solution (0.1 N) and, using the absorbance values, Chl-*a* concentrations are finally calculated (LORENZEN *et al.*, 1967).

SPM concentrations, as well as organic (OSM) and inorganic suspended matter (ISM) fractions were obtained according to the American Public Health Association protocol (APHA, 1998). Samples were filtered on the day of collection and filters were kept refrigerated until further procedures. The filters were then dried in the oven at 100°C for 12 hours, weighted using an analytical balance and, after that, taken to muffle furnace at 550° for 30 minutes and again weighted. The first weights are used for determining SPM concentration, by subtracting the value from the filter weight before the filtration; the second ones determine ISM, also by subtracting from the original weight before filtration. OSM concentrations are obtained by the difference between SPM and ISM weights.

4.2.2. Absorption coefficients

Absorbance of water samples filtered through GF/F Whatman fiberglass filters – 0.7 μm porosity – and sequentially filtered through Whatman nylon membrane – 0.22 μm porosity and 47 mm diameter – were read using a 2600 UV-VIS spectrophotometer (Shimadzu, Japan). The results were applied to calculate CDOM absorption coefficients (a_{CDOM}, m^{-1}) as proposed by Bricaud *et al*. (1981) (Eq. 3).

$$a_{CDOM} = 2.3\frac{OD_{CDOM}(\lambda)}{r} \quad \text{(Eq.3)}$$

where $OD_{CDOM}(\lambda)$ is the optical density of CDOM and r is the cuvette path length (0,1m).

In order to determine the total particulate (algal and detritus) absorption coefficients (a_p, m^{-1}), GF/F Whatman fiberglass filters – 0.7 μm porosity and 47 mm diameter – , previously used for filtering water samples, were used for reading optical density of total particulate using a double-beam 2600 UV-VIS spectrophotometer equipped with an integrating sphere. Transmittance-Reflectance method (T-R) described by Tassan and Ferrari (1995, 1998) was employed. For eliminating pigments influence, a 10% sodium hypochlorite (NaCLO) solution was applied in the filters and optical density now corresponding to detritus was measured, also through T-R technique. The spectral sampling ranged from 280 nm to 800 nm, with spectral resolution of 1 nm. From these measurements it was possible to calculate detritus absorption coefficients (a_d, m^{-1}) and a_p according to Eq. 4:

$$a_{p,d}(\lambda) = \frac{2.303\ OD_{p,d}(\lambda)}{V.A} \quad \text{(Eq. 4)}$$

where $OD_p(\lambda)$ is the optical density of total particulate; $OD_d(\lambda)$ is the optical density of detritus, V is the filtered volume (m^3) and A is the filter clearance area (m^2). Phytoplankton absorption coefficients (a_ϕ, m-^{1}) are obtained by subtracting a_d from a_p. Finally, a_{CDOM} was added to a_d in order to obtain a_{CDM}, since QAA approach derives a_{CDOM} and a_d as this combined coefficient.

4.2.3. Radiometric Data

In situ data collection also included radiance and irradiance measurements using three RAMSES sensors (TriOS, Oldenburg, Germany), operating in a spectral range between 350 and 900 nm, with spectral resolution of 3.3 nm. RAMSES-ACC measured downwelling irradiance ($E_d(\lambda)$; W m^{-2} nm^{-1}) and two RAMSES-ARC sensors measured total upwelling radiance ($L_t(\lambda)$; W m^{-2} sr^{-1} nm^{-1}) and atmospheric diffuse radiance ($L_s(\lambda)$; W m^{-2} sr^{-1} nm^{-1}). The acquisition geometry followed Mobley (1999), with $L_t(\lambda)$ measured at a zenith angle (θ) of 140° and azimuth angle (ϕ) of 90°, $L_s(\lambda)$ measured at θ of 40° and ϕ of 90°, and $E_d(\lambda)$ measured at θ of 0°, i.e. sensor aligned to Zenith, and ϕ of 90°.

Remote sensing reflectance ($R_{rs,}$ sr^{-1}) spectra was then calculated from these radiometric quantities, using spectral optimization approach proposed by Lee *et al.* (1999) as follow:

$$R_{rs}(\lambda) \approx T_{rs}(\lambda) - F(\theta) \times S_{rs}(\lambda) - \Delta \qquad \text{(Eq. 5)}$$

where $T_{rs}(\lambda)$ is the total remote sensing reflectance, which is the ratio of $L_t(\lambda)$ to $E_d(\lambda)$; $F(\theta)$ is the surface Fresnel reflectance based on the viewing geometry (~0.021); $S_{rs}(\lambda)$ is the sky remote sensing reflectance, the ratio of surface-reflected radiance ($L_r(\lambda)$) to $E_d(\lambda)$; and Δ is a spectrally constant offset for adjusting sun glint effects from $L_t(\lambda)$ measurements. Although for oceans Δ can be considered as zero in the near-infrared, in turbid waters it is significant. The absorption caused by SPM decreases to almost zero at wavelengths longer than 700 nm, and the increase of SPM concentration create a gradient in the near-infrared of R_{rs} due to the particle scattering (DEKKER, 1993; GOODIN *et al*., 1993; YANG *et al*., 2013). For obtaining Δ, R_{rs} can be modeled as a function of spectral IOPs and compared with R_{rs} calculated from above-surface measurements and, then, Δ is estimated through optimization that minimizes the error between the modeled R_{rs} and the optimized R_{rs} (LEE *et al*. 2010).

R_{rs} obtained from *in situ* measurements are inputs for QAAs. Aiming to make its outputs comparable to satellite-derived ones, hyperspectral R_{rs} was subject to convolution, then becoming correspondent to satellite data. Spectral response functions of the first twelve bands of OLCI, on board Sentinel 3A, were used to derive band-weighted data (GORDON, 1995):

$$R_{rs}^{OLCI}(\lambda_k) = \frac{\int_{\lambda_i}^{\lambda_j} S(\lambda) R_{rs}(\lambda)}{\int_{\lambda_i}^{\lambda_j} S(\lambda)} \qquad \text{(Eq. 6)}$$

where R_{rs}^{OLCI} stands for the remote sensing reflectance convoluted from OLCI spectral bands; λ_i and λ_j are the lower and upper limit of the band λ_k, respectively; and $S(\lambda)$ is the spectral response function of the *i*th spectral band of OLCI.

It is important to highlight that OLCI was still not operating when the first field campaign (IBI1) was performed and, therefore, we only had OLCI image matching to field campaign available for IBI2.

4.2.4. QAA context

QAA_{V6} (LEE, 2014), a re-design from the previous QAA original version – QAA_{V5} (LEE *et al.*, 2009) – was developed in order to improve its accuracy in water systems in which R_{rs} at 670 nm is greater than 0.0015 sr^{-1}, i.e., coastal regions and areas with high sediment concentration. Both QAA_{V5} and QAA_{V6} were used for composing the schemes for Chl-*a*

retrieval. QAA_{BBHR} (WATANABE *et al*., 2016) and QAA_{OMW} (RODRIGUES, 2017), re-parameterized versions for reservoirs located at Tietê River cascading system were also tested for the schemes.

Barra Bonita, reservoir for which QAA_{BBHR} was parameterized, is a eutrophic environment located upstream from Ibitinga reservoir and presents a broad range of Chl-*a* concentrations, with OSM corresponding to approximately 90% of total SPM (WATANABE *et al*., 2016). Nova Avanhandava Reservoir, located downstream from Ibitinga, was the basis for QAA_{OMW} parameterization. Contrasting with Barra Bonita, this reservoir presents oligo to mesotrophic waters, with low average Chl-*a* concentration, as well as low average SPM concentration in the dataset considered for the parameterization; inorganic fraction is usually predominant in total SPM (RODRIGUES, 2017).

4.2.5. Calibration and validation of absorption coefficients based models

Absorption coefficients based models for Chl-*a* concentration retrieval were calibrated for the study area. Firstly, R_{rs} spectra from 29 samples obtained in IBI1 field campaign and resampled for OLCI bands, were used as inputs for the four QAA versions aforementioned. Outputs from each QAA - a_ϕ and a_{CDM} at different wavelengths - were applied to obtain four indexes, which were subsequently used to calibrate the models. Therefore, each QAA version originated four indexes and, consequently, four models. The three first indexes, here labeled γ_1, γ_2 and γ_3 (Eqs. 7, 8, 9) are based on two-band (2B) (DEKKER, 1993), three-band (3B) (DALL'OLMO and GITELSON, 2005; GITELSON *et al*., 2008) and four-band (4B) (LE *et al*., 2009b) approaches, and were adapted by Le *et al*. (2013) in terms of a_ϕ and pure water absorption coefficient (a_w); the remaining one (γ_{NDCI}; Eq. 10) is an adaptation in terms of a_ϕ, a_w and a_{CDM} of the Normalized Difference Chlorophyll Index (NDCI) (MISHRA and MISHRA, 2012) proposed by Watanabe *et al*. (2016). Original indexes use R_{rs} at different wavelengths as inputs.

$$\gamma_1 = \frac{a_\phi(665) + a_w(665)}{a_w(709)} \qquad \text{(Eq. 7)}$$

$$\gamma_2 = \frac{a_\phi(665) + a_w(665) - a_w(709)}{a_w(754)} \qquad \text{(Eq. 8)}$$

$$\gamma_3 = \frac{a_\phi(665) + a_w(665) - a_w(681)}{a_w(754) - a_w(709)} \qquad \text{(Eq. 9)}$$

$$\gamma_{NDCI} = \frac{a_w(665) + a_\phi(665) - a_w(709)}{a_w(665) + a_{CDM}(665) + a_\phi(665) + a_w(709) + a_{CDM}(709)} \qquad \text{(Eq. 10)}$$

Using Chl-*a* concentrations from IBI1 as response variable, and γ_1, γ_2, γ_3 and γ_{NDCI} as explanatory variables – one index for each model – four models were adjusted through linear regression. In addition, each index was calculated from absorption coefficients originating from the four QAA versions and, thus, sixteen schemes – four QAA versions plus four models – were configured in total. Leave-one-out cross-validation method was used for checking representativeness of the schemes. After validation was done, accuracy of the models was assessed in order to verify which models could be applied in the image. Figure 8 (a) shows the steps for models calibration and validation.

4.2.6. Chl-a retrieval via OLCI image

A cloud free OLCI full resolution Level-1 image acquired in June 21, 2017, matching IBI2 fieldwork date, was selected. Using R_{rs} spectra collected in IBI2 and convolved for OLCI bands, empirical line (EL) atmospheric correction (KRUSE *et al*., 1990) was applied in order to obtain bottom of atmosphere R_{rs} from image top of atmosphere (TOA) radiance. In sequence, the schemes that presented reasonable performances in the cross-validation were applied to the image. Firstly, QAA were applied in the image and, then, the absorption coefficients (a_ϕ and a_{CDM}) resulting from it, were used to calculate γ_1, γ_2, γ_3 and γ_{NDCI} indexes. These calculated indexes, applied to the models previously calibrated for the study area, resulted in Chl-*a* concentration estimates in the image. Figure 8 (b) shows the steps for image processing.

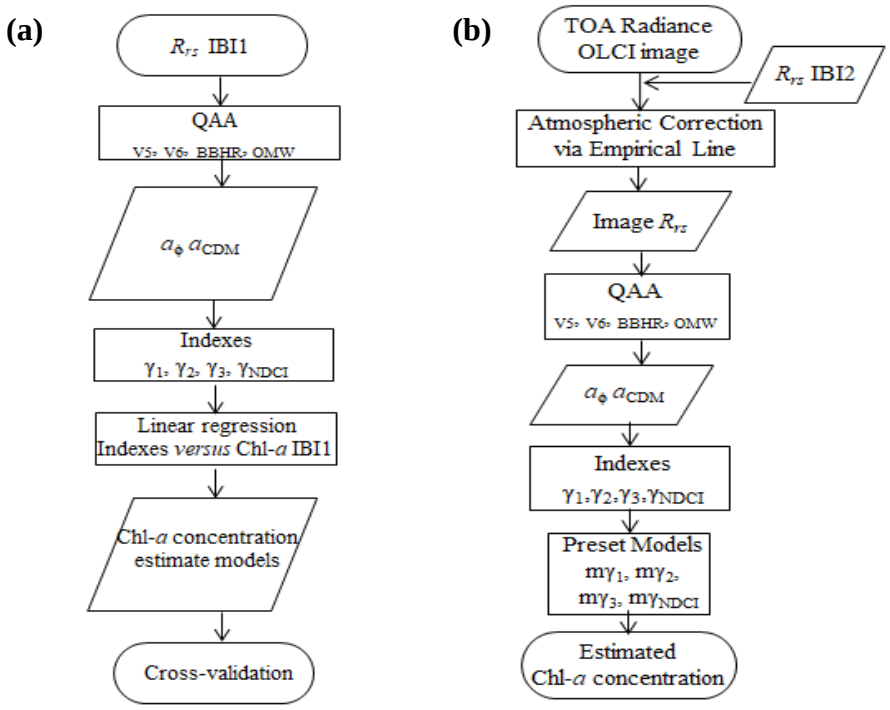

Figure 8. Flowcharts of (a) calibration process of sixteen Chl-*a* retrieval models for the study area; (b) image pre-processing and application of schemes for Chl-*a* concentration retrieval.

4.2.7. Accuracy assessment

Averaged unbiased absolute percentage difference (ε, Eq. 11) and normalized root mean square error (nRMSE, Eq. 12) were used to (i) evaluate the absorption coefficients based models after validation, (ii) to assess OLCI image atmospheric correction and also (iii) to assess Chl-*a* retrieval schemes performance for the study area via OLCI image. Reference data for accuracy assessment of each step were, respectively, Chl-*a* concentrations from IBI1, R_{rs} from IBI2 resampled for OLCI bands and Chl-*a* concentrations from IBI2.

$$\varepsilon = \left[\frac{1}{n}\sum \frac{|x_{estimated} - x_{measured}|}{x_{estimated} + x_{measured}}\right] \times 200\% \qquad \text{(Eq. 11)}$$

$$nRMSE = \frac{\sqrt{\frac{\sum (x_{estimated} - x_{measured})^2}{n}}}{x_{measured}^{max} - x_{measured}^{min}} \times 100\% \qquad \text{(Eq. 12)}$$

where n is the number of samples; $x_{\text{estimated}}$ and x_{measured} are the estimated and measured values, respectively; $x_{measured}^{max}$ and $x_{measured}^{min}$ are respectively the maximum and minimum measured values.

4.3. Results

4.3.1. Water quality characterization

Chl-*a* concentrations presented broad variation in IBI1, while in IBI2 both the range and the concentration values were lower (Table 4). SPM concentrations were higher in IBI1, as well as turbidity values. Organic and inorganic fractions of SPM presented the same trend in both datasets, with the organic matter being predominant; the second fieldwork, however, showed greater percentage of OSM. Variation of conductivity values was much higher in the second dataset, while the first one showed greater fluctuation for turbidity and also presented wider ranges of Secchi depth. Table 4 presents descriptive statistics of biogeochemical data from both field campaigns.

Table 4. Descriptive statistics of water quality data from IBI1 and IBI2 field campaigns. Min: minimum; Max: maximum; SD: standard deviation; CV: coefficient of variation; n = 29 for IBI; n = 6 for IBI2.

		Chl-*a* (mg m^{-3})	SPM (g m^{-3})	OSM/SPM	ISM/SPM	Conductivity (µs cm^{-1})	Turbidity (NTU)	Secchi Depth (m)
IBI1	**Min**	1.37	1.00	0.29	0.12	171.00	2.82	1.6
	Max	119.04	8.10	0.88	0.71	198.30	8.87	3.2
	Mean	19.34	2.45	0.63	0.37	185.71	4.24	2.23
	SD	24.71	1.40	0.15	0.15	8.37	1.19	0.35
	CV (%)	127.8	57.19	23.28	40.11	4.51	28.01	15.5
IBI2	**Min**	2.73	0.30	0.67	0.13	155.30	2.63	1.90
	Max	13.38	2.20	0.88	0.33	205.00	3.60	2.80
	Mean	9.97	1.25	0.76	0.24	170.53	3.06	2.31
	SD	4.35	0.66	0.09	0.09	19.50	0.33	0.33
	CV (%)	43.62	52.52	12.33	39.55	11.43	10.78	14.40

4.3.2. Bio-optical characterization

Descriptive statistics of absorption coefficients from IBI1 and IBI2 are shown in Table 5. In both field campaigns a_{CDM} was the absorption coefficient that presented the highest average value at 443 nm ($a_{CDM}(443)$) and, although the maximum value was much higher in IBI1, average values were similar in both datasets. $a_{CDOM}(443)$ showed the same tendency as $a_{CDM}(443)$, with substantially lower maximum values in IBI2 and very similar mean values. $a_\phi(443)$ and $a_d(443)$ average values, as well as their maximum, presented drastic reduction from IBI1 to IBI2. Variation of all absorption coefficients was much higher in the first dataset.

Table 5. Descriptive statistics of absorption coefficients from IBI1 and IBI2 field campaigns. Min: minimum; Max: maximum; SD: standard deviation; CV: coefficient of variation; n = 29 for IBI; n = 6 for IBI2.

		Minimum	**Maximum**	**Mean**	**SD**	**CV (%)**
IBI1	$a_\phi(443)$ (m^{-1})	0.06	1.88	0.30	0.36	120.44
	$a_{CDM}(443)$ (m^{-1})	1.24	5.93	1.95	0.83	42.41
	$a_d(443)$ (m^{-1})	0.14	0.62	0.37	0.13	33.54
	$a_{CDOM}(443)$ (m^{-1})	0.87	5.31	1.57	0.80	50.85
IBI2	$a_\phi(443)$ (m^{-1})	0.05	0.13	0.11	0.03	26.92
	$a_{CDM}(443)$ (m^{-1})	1.27	1.99	1.69	0.28	27.04
	$a_d(443)$ (m^{-1})	0.15	0.19	0.18	0.02	9.30
	$a_{CDOM}(443)$ (m^{-1})	1.12	1.79	1.51	0.27	17.74

Average a_ϕ, a_d and a_{CDOM} for IBI1 and IBI2 are shown in Figure 9; a_w (POPE and FRY, 1997) is also shown in order to assist analysis of total contribution of the absorption budget throughout the spectrum. It is possible to observe a_{CDOM} is dominant in the blue, green and red spectral regions of IBI2 (Figure 9 (b)); this trend was also observed by Andrade *et al*. (2017, submitted) in IBI1 (Figure 9 (a)), although a_w becomes the greater contributor above 660 nm in this dataset. In IBI2, a_d contribution is the second highest value in the blue-green region, even though the difference from a_ϕ is really modest. The difference of a_d and a_ϕ contributions is more distinct in IBI1, but a_d also contributes more than a_ϕ, as already shown by Andrade *et al*. (2017, submitted). In the red channel, a_ϕ and a_d presented similar contributions in both datasets, with minor a_ϕ increase from around 660 nm to 700 nm in both cases; this feature is more clearly seen in IBI1.

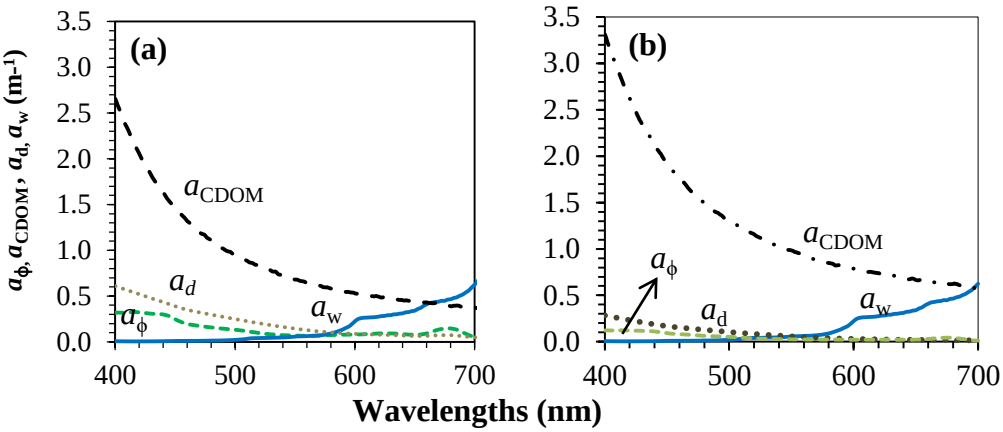

Figure 9. Average phytoplankton (a_ϕ), CDOM (a_{CDOM}), detritus (a_d) and pure water (a_w) absorption coefficients in Ibitinga reservoir in (a) IBI1 (July, 2016; *n*=29); (b) IBI2 (June, 2017; *n*=6).

R_{rs} spectra obtained from the two fieldwork measurements (Figure 10) present a peak in the green region, at approximately 550 nm, that can be related to scattering caused by inorganic suspended matter (HAN and RUNDQUIST, 1997) and low Chl-*a* absorption. Although this feature is noticeable in the spectra, its magnitude is relatively low in IBI2. It is also possible to observe features related to Chl-*a*, as the absorption feature at around 675 nm and reflectance peak at around 700 nm, which are more evident in IBI1 spectra. A discrete reflectance feature occurs around 750 nm in both datasets, followed by a minor dip at 760 nm that can possible be related to absorption by atmospheric oxygen (GOWER *et al*., 2005). R_{rs} spectra from IBI1 (already shown by ANDRADE *et al*., 2017, submitted) present, in general, slightly higher magnitudes when compared with IBI2.

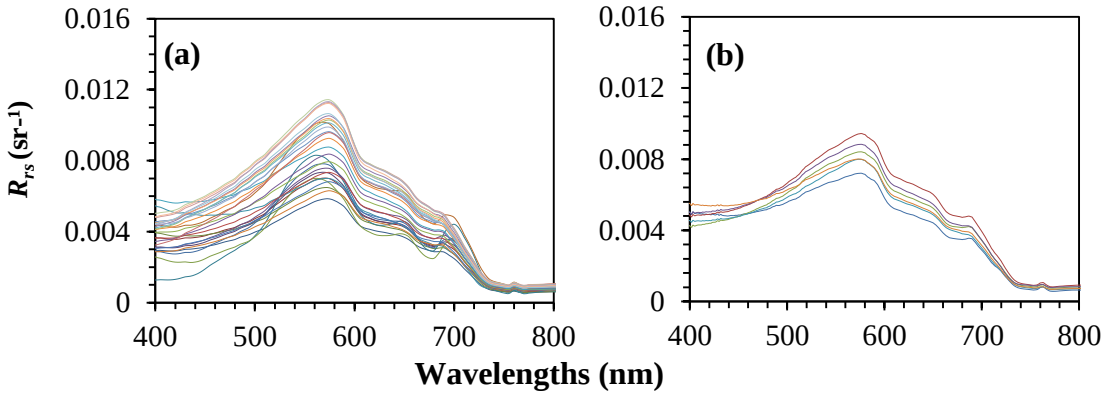

Figure 10. R_{rs} spectra obtained from *in situ* measurements in: (a) IBI1 field campaign (*n*=29); (b) IBI2 field campaign (*n*=6).

Measured R_{rs} spectra after convolution to match OLCI bands can be visualized in Figure 11. It is possible to observe that the reflectance peak at ~550 nm is preserved after the convolution. Chl-*a* features, however, were significantly softened.

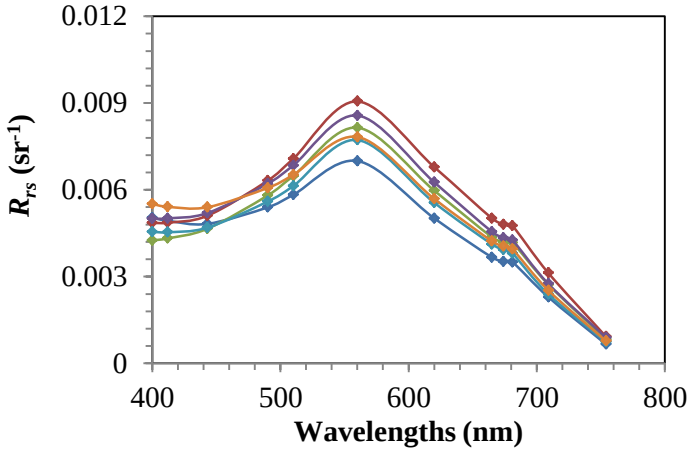

Figure 11. R_{rs} spectra from IBI2 (June, 2017, *n*=6) simulated for OLCI first twelve bands.

4.3.3. Validation of Chl-a concentration retrieval schemes

The four models calibrated for the study area using Chl-*a* concentration from IBI1 and γ_1, γ_2, γ_3 and γ_{NDCI} indexes, through linear regression, are labeled respectively as $m\gamma_1$, $m\gamma_2$, $m\gamma_3$ and $m\gamma_{NDCI}$. Each scheme – QAA plus models originated from its output – was cross-validated and the results can be visualized in Table 6; $m\gamma_1$, $m\gamma_2$ and $m\gamma_3$ presented minimal difference between its errors and, thus, are displayed together. QAA_{BBHR} plus $m\gamma_{NDCI}$ presented the lowest nRMSE and ε, although all schemes showed reasonable errors (nRMSE < 27.00%; ε < 3.50%)

Table 6. Errors between fits from cross-validated models and Chl-*a* concentrations from IBI1.

	QAA_{V5}		**QAA_{V6}**		**QAA_{BBHR}**		**QAA_{OMW}**	
	$m\gamma_1$,$m\gamma_2$, $m\gamma_3$	$m\gamma_{NDCI}$	$m\gamma_1$,$m\gamma_2$, $m\gamma_3$	$m\gamma_{NDCI}$	$m\gamma_1$,$m\gamma_2$, $m\gamma_3$	$m\gamma_{NDCI}$	$m\gamma_1$,$m\gamma_2$, $m\gamma_3$	$m\gamma_{NDCI}$
***n*RMSE (%)**	22.16	18.17	24.25	24.21	11.58	11.46	24.73	26.89
ε (%)	2.36	2.27	3.03	3.03	1.21	1.30	2.81	3.13

Considering that the four models originated from a same QAA version consistently presented similar errors, t-test for paired samples was applied and it was verified their

statistically equality (α=0.05; *p*-value=1). As the models were proven to obtain analogous results, allied to the fact that all schemes demonstrated acceptable errors after cross-validation, all of them were employed in the next processing step.

4.3.4. Atmospheric Correction Assessment

OLCI-derived R_{rs} after EL atmospheric correction were assessed based on R_{rs} obtained from IBI2 measurements and resampled for OLCI bands (Figure 12 (a)); errors referrers to the average for all IBI2 sampling stations. The highest errors (nRMSE and ε) occurred at 412 nm.

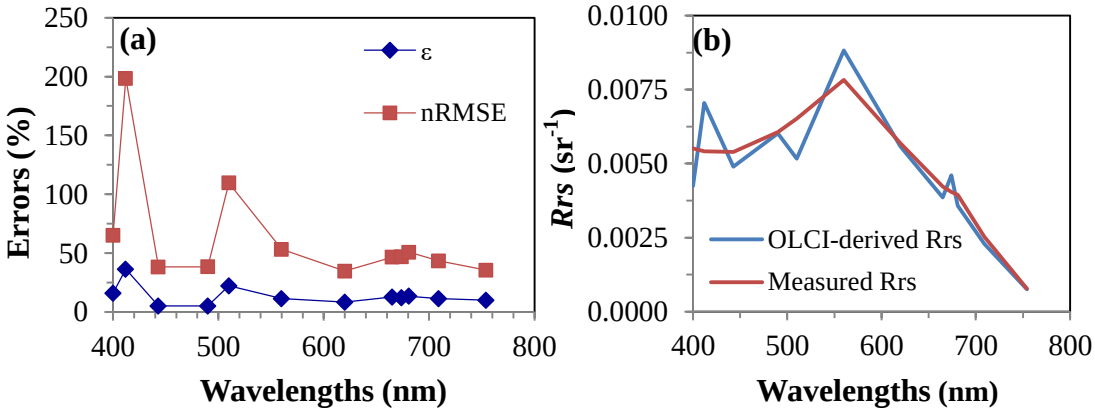

Figure 12. (a) Errors between OLCI-derived R_{rs} spectra after Empirical Line (EL) atmospheric correction *versus* R_{rs} spectra from field campaign (IBI2) measurements resampled for OLCI bands (average for all sampling stations). (b) Comparison of OLCI-derived R_{rs} spectrum after atmospheric correction and R_{rs} spectrum from IBI2 measurements resampled for OLCI bands at sampling station 6. First twelve OLCI bands are shown in both (a) and (b).

On the other hand, the lowest nRMSE occurred at 620 nm (34.77%), while ε was lowest at 443 nm (5.05%). Most bands presented nRMSE ranging from ~35 to ~53% and ε from ~5 to ~16%. Regarding all bands, average nRMSE was 63.41% and average ε was 13.64%. Bias (not shown here) ranged from -0.0013 to 0.0021 m^{-1}, with negative values in the majority of the wavelengths analyzed, which means that the empirical line method presented a trend of underestimating R_{rs} values.

Figure 12 (b) shows OLCI-derived R_{rs} spectrum after EL atmospheric correction and R_{rs} spectrum from IBI2 fieldwork at a unique sampling station (station 6). Overall, it presents the same tendency that can be seen in Figure 12 (a), with major discrepancies occurring in the blue channel, while the red spectral region presents minor ones.

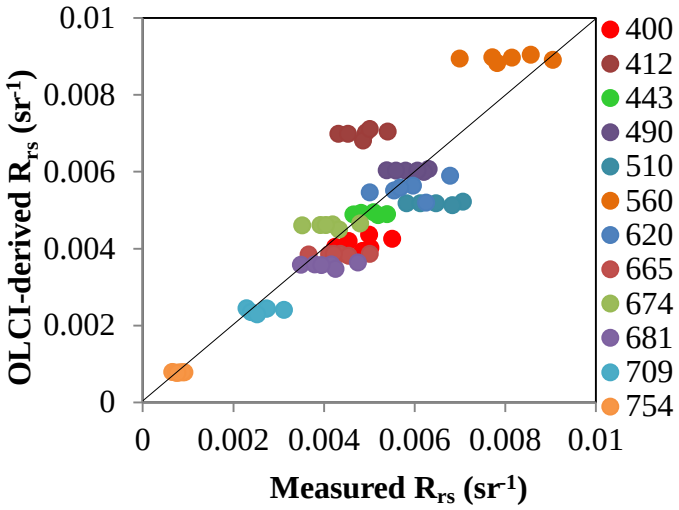

Figure 13. Comparison per band of *in situ* R_{rs} and OLCI-derived R_{rs} after Empirical Line atmospheric correction; six satellite-*in situ* matchups are considered.

Comparing, per band, OLCI-derived R_{rs} after atmospheric correction and R_{rs} calculated from *in situ* measurements (Figure 13), it can be observed that values from 412 nm band were consistently overestimated and are the most discrepant ones. 560 nm band also presents most of values overestimated, while the majority of other bands presents a slight underestimating trend.

4.3.5. Assessment of Chl-a Retrieval via OLCI image

After applying all schemes – QAA plus model – in the image already atmospherically corrected, the accuracy of Chl-*a* concentration estimates retrieved from each scheme was assessed using Chl-*a* concentrations obtained in IBI2. The QAA_{V5} plus $m\gamma_{NDCI}$ scheme presented the best results – nRMSE of 42.42% and ε of 37.82% – while the other models ($m\gamma_1$, $m\gamma_2$, $m\gamma_3$) tested with QAA_{V5} outputs showed slight greater errors (Table 7). Despite that, all QAA_{V5} schemes presented the lowest errors when compared with schemes using other QAA versions. Only QAA_{V5} based schemes presented reasonable results, since all schemes based on other QAA versions presented nRMSE greater than 287.29 % and ε greater than 122.96%.

Table 7. Models performances for indexes estimated via QAA_{V5} applied in the image.

	$m\gamma_{NDCI}$	$m\gamma_1$	$m\gamma_2$	$m\gamma_3$
***n*RMSE (%)**	42.42	47.48	46.36	46.36
ε (%)	37.82	39.59	38.76	38.76

Models set through linear regression, using indexes obtained via QAA_{V5} outputs and Chl-*a* concentrations from IBI1 are displayed in Figure 14. $m\gamma_{NDCI}$ presents the highest R^2 (0.5592), although other models also show R^2 around 0.5. Considering all schemes (not shown), QAA_{BBHR} plus $m\gamma_{NDCI}$ demonstrated the best fit, with R^2 of ~0.84; however, as already explained, QAA_{BBHR} schemes did not present good results for image data (corresponding with IBI2), despite of the great fits of the models for IBI1 data.

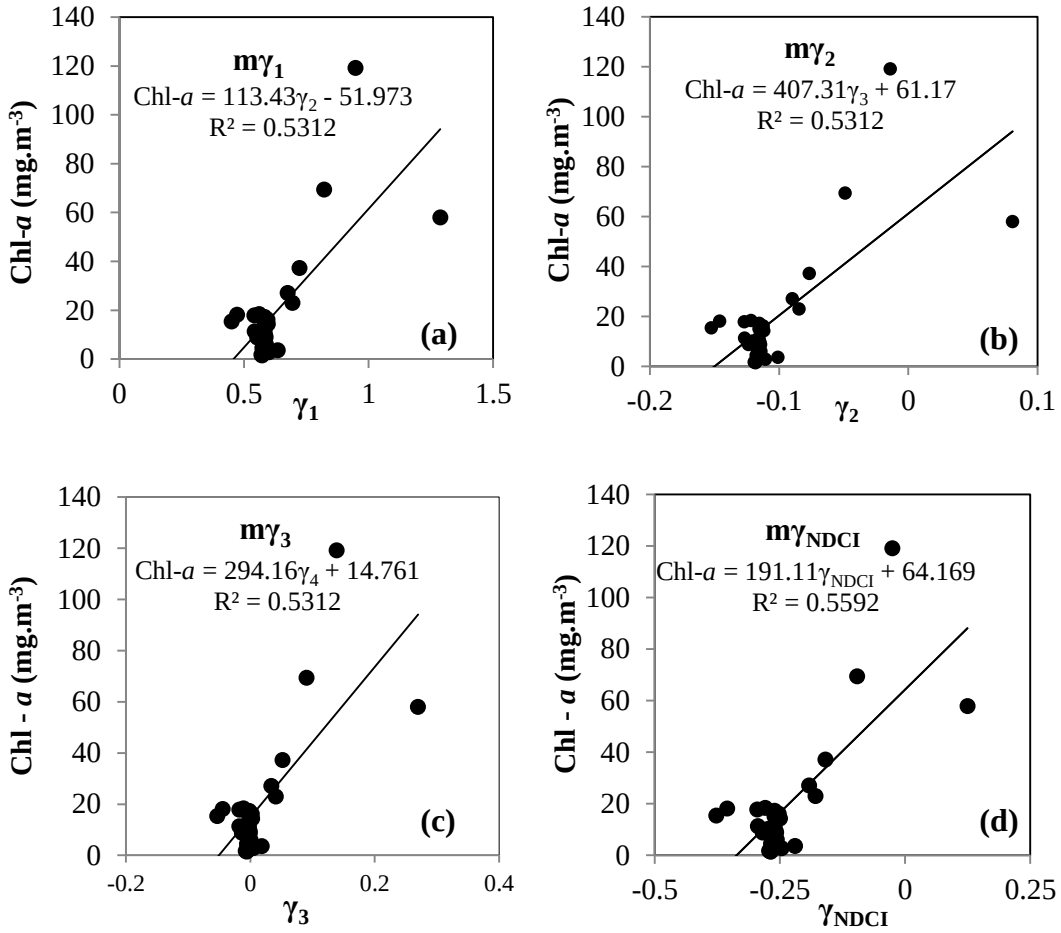

Figure 14. Models configured from (a) γ_1 ($m\gamma_1$); (b) γ_2 ($m\gamma_2$); (c) γ_3 ($m\gamma_3$); and (d) γ_{NDCI} ($m\gamma_{NDCI}$). Indexes used QAA_{V5} outputs.

Chl-*a* concentrations obtained via QAA_{V5} based schemes are shown in Figure 15, since these schemes were the only ones able to retrieve reasonable accurate estimates (nRMSE < 47.50% and ε < 39.60%). It can be verified in the images that tributaries rivers present low Chl-*a* concentrations when comparing to concentrations from the main body of the reservoir. Since average Chl-*a* concentration in the sampling stations was ~ 10 mg m^{-3} in IBI2 dataset, and in the image these stations are mostly located at yellow areas (~ 13 mg m^{-3}), it is possible to infer that the schemes slightly overestimated the concentrations. It is

also possible to observe that station 4 is located at a yellow to red transition region and it is actually the higher concentration station.

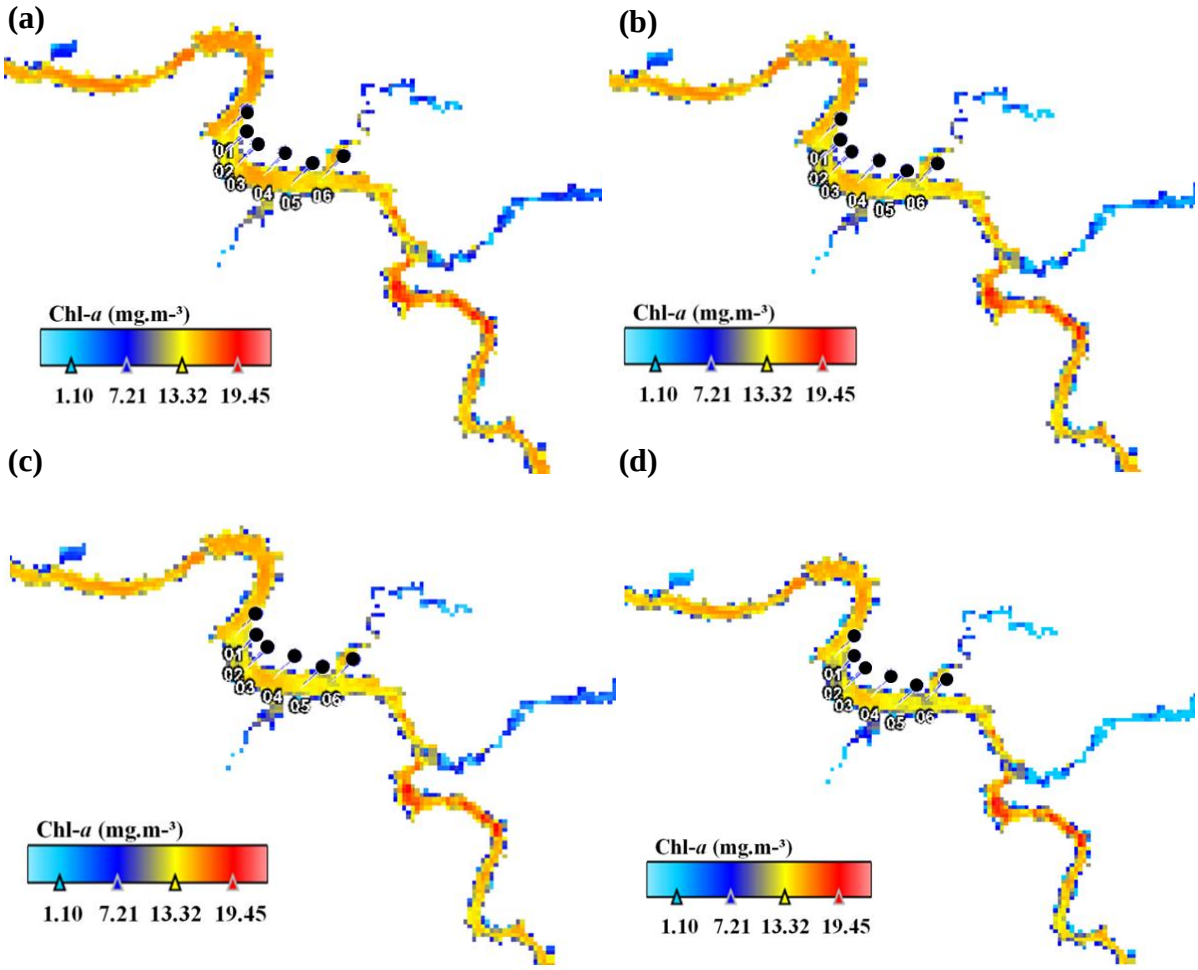

Figure 15. Spatial distribution of Chl-*a* concentrations in Ibitinga Reservoir using OLCI image acquired on June 21st, 2017. Chl-*a* retrieved via (a) QAA_{V5} plus $m\gamma_1$ scheme; (b) QAA_{V5} plus $m\gamma_2$ scheme; (c) QAA_{V5} plus $m\gamma_3$ scheme; (d) QAA_{V5} plus $m\gamma_{NDCI}$ scheme.

4.4. Discussion

Water quality data analysis shows not only significant variability within each fieldwork dataset, but also a huge variability of values and amplitudes of most parameters from one field campaign to another. Water quality data analysis shows not only significant variability within each fieldwork dataset, but also a huge variability of values and amplitudes of most parameters from one field campaign to another. These observations may be related to two main factors: the water residence time and precipitation rates preceding the data collection, elements which are also related to each other.

Water residence time varies cyclically over time, affecting the nutrients concentration and, consequently, the trophic state in a reservoir (LONDE *et al*., 2016; VIEIRA *et al*., 2002); according to Vieira *et al*. (2002), water residence time in IHR is relatively short, what leads to more frequents nutrients cycling. Considering that the data collections occurred after different precipitation amounts in the region – the first fieldwork was carried out after a period of low precipitation rates, while the second occurred after considerable precipitation amounts (NASA/GIOVANNI, 2016, 2017) –, it possible affected the water residence time, that may have been longer during the first data collection, what triggered higher nutrients concentration and, consequently, may have caused phytoplankton proliferation in more intense rates. In the other hand, the second data collected presented lower values for water quality parameters, what may be related to the precipitations amounts leading to a shorter residence time, and reduced nutrients availability and, then, fewer occurrences of phytoplankton blooms.

Vieira *et al*. (2002) also observed that the limnological variables were influenced by the location of the sampling stations, supporting the fact that spatial variations are standard in IHR. It can be related, for example, to the distinct contribution arriving from the watershed; IHR presents a narrow and prolonged shape, similar to a river channel, extending in 70 km along Tietê River, and this significant spatial distribution may contribute to different inputs to be introduced.

When it comes to bio-optical data, although the proportions of absorption coefficients were kept similar, the ranges varied considerably when comparing IBI1 and IBI2 data. Even when data from the same six stations sampled in both fieldworks are compared, the variability keeps substantial. R_{rs} spectra from both datasets presented similar features, except for the more prominent Chl-*a* absorption features observed in few IBI1 spectra, related to higher Chl-*a* concentrations observed in some stations during the first field campaign (ANDRADE *et al*., 2017, submitted), that were not present in IBI2. However, the spectra magnitudes changed

from IBI1 to IBI2, with IBI1 presenting the higher ones, as shown by Andrade *et al*. (2017, submitted). This verification correlates to data displayed in Table 1, since water quality parameters demonstrated greater values in IBI1. Besides that, the relatively low magnitude of the reflectance peak at around 550 nm, associated to inorganic suspended matter, also correlates with data shown in Table 1, in which ISM is not the major constituent of SPM. Summarizing, biogeochemical and optical parameters in Ibitinga Reservoir showed to be widely changeable, presenting significant variability in both spatial and temporal spheres.

It is important to point that Chl-*a* absorption features around 675 nm in R_{rs} spectra were substantially smoothed after resampling process, and this can have implications in the next steps of Chl-*a* estimation. Empirical line atmospheric correction performed relatively well for this case, with great fits in red channel. Since this spectral region, in special 665 nm, is key for Chl-*a* diagnosis, the reasonable resultant errors after atmospheric correction (nRMSE of 46.52% and ε of 12.71% at 665 nm) are fundamental for good results in next steps of Chl-*a* retrieval. On the other hand, the high errors occurred at 412 nm are a significant limitation; 412 nm band is directly used for $a_{CDM}(443)$ and, subsequently, $a_{CDM}(\lambda)$ estimation in QAA and, except for QAA_{OMW} version, $a_{\phi}(\lambda)$ is derived from $a_{CDM}(\lambda)$ estimates. Shen *et al*. (2017) used the Second Simulation of the Satellite Signal in the Solar Spectrum correction scheme (6S model) for atmospheric correction of OLCI images for investigating a turbid and eutrophic lake in China, and found an average nRMSE around 50.00% for all bands, presenting only a minor difference from the average nRMSE showed by the empirical line atmospheric correction in this study (nRMSE of 63.41%). A research carried out in coastal waters of the Baltic Sea, used the Case-2 Regional/Coast Colour (C2RCC) processor for atmospheric correction of OLCI image and it presented a reasonable performance, although the blue spectral region presented major issues – just as it was found in this study (TOMING *et al.*, 2017). According to the authors, it probably occurred because atmospheric and glint effects are higher in the blue part of the spectrum and, thus, atmospheric correction of these bands are indeed more difficult.

Regarding the suitability of QAA plus absorption coefficients based models schemes for the study area, the models based on absorption coefficients originating from QAA_{BBHR} showed the highest R^2. Also, QAA_{BBHR} based schemes presented lower errors after leave-one-out cross-validation, being QAA_{BBHR} followed by $m\gamma_{NDCI}$ the one with the lowest errors. Although the great performances regarding IBI1 dataset, QAA_{BBHR} did not present even reasonable results in the image, for which it presented negative estimates for a_{ϕ}.

The considerable variability in the reservoir is a potential explication for these facts. Since the environment scenario hugely changed from the first fieldwork to the second one, QAA_{BBHR} parameterization was not the one that best reflected the reservoir characteristics. The fact that QAA_{BBHR} was developed considering the phytoplankton features of Barra Bonita reservoir, a eutrophic water system, allied to the observation that IBI1 dataset comprised really higher Chl-*a* concentration helps understanding why QAA_{BBHR} performance was better for IBI1, but not appropriate for the image data – acquired during an apparently low Chl-*a* concentration period.

Differently of what could have been expected, QAA versions parameterized for reservoirs in the same cascading system did not perform well for Ibitinga, what indicates variability along the system. QAA_{V5} presented the best results for $a_\phi(665)$ in IBI1 (nRMSE of 15.35%), as reported by Andrade *et al*. (2017, submitted). Considering that $a_\phi(665)$ is an input for the calculation of all four indexes used in the absorption coefficients based models, it is an important observation that possibly explains the good results of QAA_{V5} schemes applied in the image data. Since a dataset different from the one used for models calibration was being considered, R^2 and cross-validation results are not the best indicators for explaining schemes efficiency – what explains the apparent divergence of QAA_{BBHR} performances. When analyzing $a_{CDM}(665)$ and $a_{CDM}(709)$, both used for γ_{NDCI} calculation, QAA_{V5} estimated these coefficients with nRMSE of, respectively, 22.42% and 21.65% in IBI1. This performance is really similar to the ones presented by the other three QAA versions tested for IBI1. The errors values are reasonable and indicate the potential of QAA_{V5}, as well as other versions, in estimating a_{CDM} for the study area. When it comes to absorption coefficients retrieval for IBI2 dataset, QAA_{V5} also performed really well for $a_\phi(665)$, confirming its suitability for retrieving a_ϕ at this wavelength in Ibitinga reservoir.

Among all absorption coefficients based models tested, the one based on NDCI – adapted for absorption coefficients input – presented slightly better results for both QAA_{BBHR} and QAA_{V5} based schemes, in the calibration, validation and application in the image. It means that this index performed well for both datasets. However, paired t-tested confirmed that all four models tested are statistically equals – means differences equal to zero (α=0.05; *p*-value=1). Mishra and Mishra (2012) reported extensive validation of the index for optically complex turbid productive waters with a variety of Chl-*a* concentration ranges, and verified its good potential. Watanabe *et al*. (2016) adapted NDCI for absorption coefficients inputs and applied it for QAA_{BBHR} derived coefficients in Barra

Bonita reservoir; the scheme tested – QAA_{BBHR} plus adapted NDCI – presented better results when compared with original NDCI performance.

When analyzing Chl-*a* spatial distribution resulted from QAA_{V5} based schemes applied to the OLCI image, it can be visualized that the reservoir presents greater concentrations when comparing to tributaries rivers. Among the several environmental changes caused by the construction of reservoirs, reduction of water residence time is a significant one, which associated to nutrients availability increase commonly caused by pollution sources, possibly explains the reservoir higher Chl-*a* concentrations (TUNDISI and MATSUMURA-TUNDISI, 2008). The color distribution within the stations is a potential indicator of schemes accuracy, since it apparently correlates to the concentrations observed in fieldwork. According to the trophic state index for Chl-*a* used as reference by the environmental agency of São Paulo State, Brazil (CETESB), the concentrations observed in the image classifies the reservoir as eutrophic in most areas (LAMPARELLI, 2004; CETESB, 2009).

4.5. Conclusions

We have assessed sixteen approaches for Chl-*a* retrieval from remote sensed data. Schemes are composed by QAA followed by models that use absorption coefficients as inputs. The schemes were applied to an OLCI image. Only QAA_{V5} based schemes could retrieve reasonable estimates for image data and the four models tested presented similar good results, being NDCI based model the one with best performance. Although the slight better results for NDCI based models, all models tested can be considered statistically equals and, thus, either of them could be used for Chl-*a* retrieval in the period in question. The potential of OLCI sensor for Chl-*a* retrieval in inland waters was confirmed and, considering its temporal (2-3 days) and spatial (300 m – full resolution) resolutions, it demonstrate to be a great tool for inland waters monitoring. Considering the Chl-*a* concentrations estimated through the image, the reservoir presented a eutrophic condition (CETESB, 2009).

The main difficulties found in the process of retrieving Chl-*a* concentration via absorption coefficients in this tropical reservoir were the huge temporal and spatial variability and, consequently, an algorithm parameterization suitable for this changeable environment. The QAA versions re-parameterized for reservoirs in the same cascading system were not suitable for Ibitinga reservoir, which presented different optical and bio-geochemical characteristics when comparing with Barra Bonita and Nova Avanhandava reservoirs. While Barra Bonita absorption is dominated by phytoplankton and Nova Avanhandava has some a_d predominance, absorption in Ibitinga reservoir showed to be dominated by CDOM. Further investigations are necessary in order to verify schemes performance in other possible environmental conditions of the Ibitinga reservoir and, prospectively, obtain a timeless Chl-*a* concentration retrieval scheme via absorption coefficients.

Acknowledgements

The authors thank FAPESP Projects (Process N° 2012/19821-1 and 2015/21586-9) and Professor Edivaldo Velini and staffs from FCA/UNESP for allowing the use of their laboratory facilities.

CHAPTER 5: FINAL CONSIDERATIONS AND RECOMMENDATIONS

The main objective proposed in this research, to obtain Chl-*a* concentrations in IHR using its absorption coefficients, was successfully achieved. All specific objectives, which include the bio-optical and bio-geochemical characterization of the reservoir, assessment of performances of QAA versions and Chl-*a* estimate models, and verification of spatial distribution of Chl-*a* via OLCI image, were also obtained.

Ibitinga reservoir presented significant variation in OSCs concentrations and absorption coefficients values in the two field campaigns carried out, although the same tendency was observed in both of them. The absorption in the reservoir showed to be dominated by CDOM and the organic matter fraction was greater in the SPM; Chl-*a* presented a wide range of concentrations, especially in the first fieldwork. In the second fieldwork, the maximum values from both absorption coefficients and OSCs concentrations considerably decreased. The study area is, therefore, subject to both spatial and temporal variability, as verified.

Regarding QAAs performances for the first dataset, all versions tested presented, in average, quite similar errors when retrieving a_ϕ in IHR and showed not to be completely suitable for the reservoir. The lowest error in 665 nm band, which is key for Chl-*a* estimation, was shown by $QAA_{V5,}$ and not by $QAA_{BBHR,}$ as previously expected. When it comes to a_{CDM} retrieval, QAA_{BBHR} also did not perform perfectly well and QAA_{OMW} presented slightly better results. At this point, part of the hypothesis was rejected, since it conjectured that QAA_{BBHR} would be able to obtain accurate estimates of a_ϕ but would not present the same good performance for a_{CDM}, while, in fact, for the first dataset it was not completely adequate for retrieving neither a_ϕ nor $a_{CDM.}$

With a second dataset available, schemes composed by QAA plus models for Chl-*a* retrieval based on absorption coefficients were assessed. After calibration using the first dataset, models were cross-validated and QAA_{BBHR} based schemes presented the lowest error. Nevertheless, when applied in the OLCI image and compared with the second dataset – data collection was coincident with image acquisition –, QAA_{BBHR} based schemes did not present a good performance. $QAA_{V5,}$ which already had shown better result for a_ϕ retrieval in 665 nm in the first dataset, was part of the only schemes able to obtain reasonable estimates of Chl-*a* concentrations in IHR, when applied in the OLCI image. Thus, the main objective proposed was completed. Since it was also hypothesized that would be possible to accurately retrieve Chl-*a* concentrations in IHR from a_ϕ retrieved from QAA_{BBHR}, this part was also rejected.

Future works must be carried out in order to better understand the variability in IHR in terms of space and time. Besides that, the already assessed QAA versions must be tested with further datasets obtained in IHR, so that would be possible to actually conclude about their suitability in the study area.

The results obtained support further works, which can prospectively, lead to many practical applications, as monitoring of trophic state in the study area from satellite data, with higher accuracy provided by the use of models that can consistently retrieve the IOPs for this specific water system. It also supply evidences for future research aiming to achieve an algorithm able to obtain IOPs and OSCs concentration in the whole Tietê River cascading system, since this study analyzes data from reservoirs situated in different locations of the cascade, as well as assess the performance of QAA versions re-parameterized for a single reservoir in the cascade in retrieving IOPs for other reservoir in the same cascading system.

REFERENCES

ALCÂNTARA, E. *et al*. An investigation into the phytoplankton package effect on the chlorophyll-*a* specific absorption coefficient in Barra Bonita reservoir, Brazil. *Remote Sensing Letters*, v. 7, n.8, p. 761-770, 2016. doi:10.1080/2150704X.2016.1185189

AMERICAN PUBLIC HEALTH ASSOCIATION (APHA). Standard Methods for the Examination of Water and Wastewater. *American Water Works Association* (AWWA), *Water Environmental Federation* (WEF). Washington, USA, 1998.

ANDRADE, C. P. *et al*. Potentials and limitations of a quasi-analytical algorithm for retrieving the water absorption properties in a cascading reservoir system. Manuscript submitted for publication, 2017.

AYRES, W. *et al*. *Integrated Lake and Reservoir Management: World Band Approach and Experience* 358. Washington, DC.: World Bank, 1996.

BARBOSA, F. A. R. *et al*. The Cascading Reservoir Continuum Concept (CRCC) and Its Application to the River Tietê-Basin, São Paulo State, Brazil. In *Theoretical Reservoir Ecology and Its Applications*, edited by J. G. Tundisi, and M. Straskraba, p. 425–437. São Carlos: International Institute of Ecology, Academy of Sciences and Backhuys Publishers, 1999.

BRICAUD, A.; MOREL, A.; PRIEUR, L. Absorption by Dissolved Organic Matter of the Sea (Yellow Substance) in the UV and Visible Domains. *Limnology and Oceanography*, v. 26, p. 43–53, 1981. doi:10.4319/lo.1981.26.1.0043

BRICAUD, A.; ROESLER, C.; ZANEVELD, J. R. V. In situ methods for measuring the inherent optical properties of ocean waters. *Limnology and Oceanography*, v. 40, n. 2, p. 393–410, 1995.

BRÖNMARK, C.; HANSSON, L.A. Environmental issues in lakes and ponds: current state and perspectives. *Environmental Conservation*, v. 29, n. 3, p. 290–306, 2002.

BUKATA, R.P. Retrospection and introspection on remote sensing of inland water quality: "Like deja vu all over again". *Journal of Great Lakes Research*, v. 39, p. 2–5, 2013. doi: 10.1016/j.jglr.2013.04.001

CAIRO, C. T. *et al*. 2017. Spatial and seasonal variation in diffuse attenuation coefficients of downward irradiance at Ibitinga Reservoir, São Paulo, Brazil. *Hydrobiologia*, v. 784, p. 265–282, 2017. doi:0.1007/s10750-016-2883-7

CARDER, K. L. *et al*. Semianalytic Moderate-Resolution Imaging Spectrometer algorithms for chlorophyll a and absorption with bio-optical domains based on nitrate-depletion temperatures. *Journal of Geophysical Research*, v. 104, n. C3, p. 5403-5421, 1999.

CARPENTER, S.R.; STANLEY, E.H.; VANDER ZANDEN, M.J. State of the world's freshwater ecosystems: physical, chemical, and biological changes. *Annu. Rev. Environ. Resour*., v. 36, p. 75–99, 2011.

COMITÊ DE BACIA HIDROGRÁFICA TIETÊ-JACARÉ (CBH-TJ). *Relatório de situação dos recursos hídricos 2013 - ano base 2012*. UGRHI 13 - Bacia Hidrográfica Tietê-Jacaré. Araraquara, 2013. Available at:

<http://www.sigrh.sp.gov.br/public/uploads/documents/7476/relatorio-de-situacao- 2013-cbh-tj.pdf>. Access on: Apr 23th, 2017.

COMPANHIA DE TECNOLOGIA DE SANEAMENTO AMBIENTAL (CETESB). Relatório de qualidade das águas interiores do Estado de São Paulo 2004. São Paulo. *Série Relatórios - Secretaria de Estado do Meio Ambiente:* 297 p. Annual Report, 2005.

COMPANHIA AMBIENTAL DO ESTADO DE SÃO PAULO (CETESB). Relatório de qualidade das águas interiores do estado de São Paulo 2008. São Paulo: *Série Relatórios - Secretaria de Estado do Meio Ambiente* 1: 531p. Annual report, 2009.

DALL'OLMO, G.; GITELSON, A. A. Effect of bio-optical parameter variability and uncertainties on the remote estimation of chlorophyll – a concentration in turbid productive waters: Experimental results. *Applied Optics*, v. 44, n. 15, p. 412-422, 2005.

DEKKER, A.G. Detection of Optical Water Quality Parameters for Eutrophic Waters by High Resolution Remote Sensing. 1993. *Thesis* (PhD Earth and Life Sciences) - Proefschrift Vrije Universiteit, Amsterdam, The Netherlands.

DELLAMANO-OLIVEIRA, M. J. *et al.* Phytoplankton Taxonomic Composition and Temporal Changes in a Tropical Reservoir. *Fundamental and Applied Limnology,* v. 171, p. 27–38, 2008. doi:10.1127/1863-9135/2008/0171-0027.

DÖRNHÖFER, K.; OPPELT, N. Remote sensing for lake research and monitoring: Recent advances. *Ecological Indicators,* v. 64, p. 105–122, 2016.

EUROPEAN SPACE AGENCY (ESA). Sentinel-3a earth colour data released. *Online.* 2016. Available on: <http://www.esa.int/Our_Activities/Observing_the_Earth/Copernicus/Sentinel-3/Sentinel-3A_Earth_colour_data_released>. Access on: May 13th, 2017.

GITELSON, A. A. The peak near 700 nm on radiance spectra of algae and water: relationships of its magnitude and position with chlorophyll concentration. *International Journal of Remote Sensing*, v. 13, n. 17, p. 3367–3373, 1992. doi:10.1080/01431169208904125.

GITELSON, A. A. *et al*. A simple semi-analytical model for remote estimation of chlorophyll-a in turbid waters: Validation. *Remote Sensing of Environment,* v. 112, p. 3582–3593, 2008. doi: 0.1016/j.rse.2008.04.015

GOLTERMAN, H. L.; CLYMO, R. S.; OHNSTAD, M. A. M. *Methods for physical and chemical analysis of fresh waters.* Oxford: Blackwell Scientific, 1978.

GONS, H. J. Optical teledetection of chlorophyll a in turbid inland waters. *Environmental Science and Technology,* v. 33, n. 7, p. 1127–1132, 1999.

GORDON, H.R. A Methodology for Dealing with Broad Spectral. *Applied Optics,* v. 34, n. 36, p. 8363–74, 1995.

GORDON, H. R.; MOREL, A. Remote assessment of ocean color for interpretation of satellite visible imagery: A review. *Coastal and Estuarine studies*, v. 4, 1 ed., New York: Springer-Verlag, 1983.

GOWER, J. F. R.; DOERFFER, R.; BORSTAD, G. A. Interpretation of the 685nm peak in water-leaving radiance spectra in terms of fluorescence, absorption and scattering, and its

observation by MERIS. *International Journal of Remote Sensing*, v. 20, n. 9, p. 1771–1786, 1999.

GOWER, J. *et al*. Detection of intense plankton blooms using the 709 nm band of the MERIS imaging spectrometer. *International Journal of Remote Sensing,* v. 26, n.9, p. 2005-2012, 2005. doi: 10.1080/01431160500075857

GUIMARÃES Jr., C. *et al*. Aspectos limnológicos do reservatório de Ibitinga – SP. *Brazilian Journal of Water Resources*, v. 3, n. 1, p. 89-103, 1998. doi:10.21168/rbrh.v3n1.p89-103

HAN, L.; RUNDQUIST, D. C. Comparison of NIR/RED ratio and first derivative of reflectance in estimating algal-chlorophyll concentration: A case study in a turbid reservoir. *Remote Sensing of Environment,* v. 62, n. 3, p. 253-261, 1997. doi:10.1016/S0034-4257(97)00106-5

KRUSE, F. A. Mineral mapping at Cuprite, Nevada with a 63 channel imaging spectrometer. *Photogrammetric Engineering and Remote Sensing,* v. 56, n. 1, p. 83-92, 1990.

LAMPARELLI, M. C. Grau de trofia em corpos d'água do estado de São Paulo: avaliação dos métodos de monitoramento. 2004. *Thesis* (PhD Sciences of aquatic and terrestrial ecosystems) - Instituto de Biociências da Universidade de São Paulo, São Paulo.

LE, C. F. *et al*. Validation of a quasi-analytical algorithm for highly turbid eutrophic water of Meiliang Bay in Taihu Lake, China. *IEEE Transactions on Geoscience and remote sensing and Remote Sensing*, v. 47, n. 8, p. 2492 – 2500, 2009a. doi:10.1109/TGRS.2009.2015658

LE, C. F. *et al*. A four-band semi-analytical model for estimating chlorophyll a in highly turbid lakes: The case of Taihu Lake, China. *Remote Sensing of Environment*, v. 113, n. 6, p. 1175- 1182, 2009b. doi: 10.1016/j.rse.2009.02.005

LE, C. F. *et al*. Evaluation of chlorophyll-a remote sensing algorithms for an optically complex estuary. *Remote Sensing of Environment,* v. 129, p. 5-89, 2013. doi:10.1016/j.rse.2012.11.001

LEE, Z. *et al*. Hyperspectral remote sensing for shallow waters: 2. Deriving bottom depths and water properties by optimization. *Applied Optics*, v. 38, n. 18, p. 3831- 3843, 1999. doi:10.1364/AO.38.003831

LEE, Z.; CARDER, K. L.; ARNONE, R. A. Deriving inherent optical properties from water color: a multiband quasi-analytical algorithm for optically deep waters. *Applied Optics*, v. 41, n. 27, p. 5755 – 5772, 2002. doi:10.1364/AO.41.005755

LEE, Z. *et al.* 2009. An update of the Quasi-Analytical Algorithm (QAA_v5). *International Ocean Color Group Software Report* (IOCCG). Available on: <http://www.ioccg.org/groups/Software_OCA/QAA_v5.pdf>. Access on: 15th June, 2017.

LEE, Z. *et al*. Removal of surface-reflectance light for the measurement of remote sensing reflectance from an above-surface platform. *Optics Express*, v. 18, n. 25, p. 26313 – 26324, 2010. doi: 10.1364/OE.18.026313

LEE, Z. 2014. “Update of the Quasi-Analytical Algorithm (QAA_v6).” *International Ocean Color Group Software Report* (IOCCG) Available on: <http://www.ioccg.org/groups/Software_OCA/QAA_v6_2014209.pdf>. Access on: 15th June, 2017.

LI, L. *et al*. An inversion model for deriving inherent optical properties of inland waters: Establishment, validation and application. *Remote Sensing of Environment*, v. 135, p. 150-166, 2013. doi:10.1016/j.rse.2013.03.031

LI, L.; LI, L.; SONG, K. Remote sensing of freshwater cyanobacteria: An extended IOP Inversion of Inland Waters (IIMIW) for partitioning absorption coefficient and estimating phycocyanin. *Remote Sensing of Environment*, v. 157, p. 9-23, 2015. doi: 10.1016/j.rse.2014.06.009

LONDE, L. R. *et al*. Water residence time affecting phytoplankton blooms: study case in Ibitinga Reservoir (São Paulo, Brazil) using Landsat/TM images. *Brazilian Journal of Biology*. v. 76, p. 664- 672, 2016.

LORENZEN, C. J. Determination of chlorophyll and pheo-pigments: Spectrophotometric equations. *Limnology and Oceanography*, v. 12, p. 343-346, 1967. doi:10.4319/lo.1967.12.2.0343

MATTHEWS, M. W. A current review of empirical procedures of remote sensing in inland and near-coastal transitional waters. *International Journal of Remote Sensing*, v. 32, n. 21, p. 6855–6899, 2011.

MISHRA, S.; MISHRA, D.R. Normalized difference chlorophyll index: a novel model for remote estimation of chlorophyll-*a* concentration in turbid productive waters. *Remote Sensing of Environment*, v. 117, p. 394 – 406, 2012. doi: 10.1016/j.rse.2011.10.016

MISHRA, S. *et al*. Quantifying cyanobacterial phycocyanin concentration in turbid productive waters: A quasi-analytical approach. *Remote Sensing of Environment*, v. 133, p. 141–151, 2013. doi:10.1016/j.rse.2013.02.004

MISHRA, S.; MISHRA, D. R.; LEE, Z. Bio-Optical Inversion in Highly Turbid and Cyanobacteria-Dominated Waters. *IEEE Transactions on Geoscience and Remote Sensing*, v. 52, n. 1, p. 375–388, 2014. doi:10.1109/TGRS.2013.2240462

MOBLEY, C. D. Estimation of the remote-sensing reflectance from above-surface measurements. *Applied Optics*, v. 38, n. 36, p. 7442-7455, 1999. doi:10.1364/AO.38007442

MOREL, A. In-water and remote measurements of ocean color. *Boundary-Layer Meteorology*, v. 18, n. 2, p. 177–201, 1980.

MOSS, B. Cogs in the endless machine: lakes, climate change and nutrient cycles: a review. *Sci. Total Environ*. v. 434, p. 130–142, 2012.

MOUW, C. B. *et al*. Aquatic color radiometry remote sensing of coastal and inland waters: Challenges and recommendations for future satellite missions. *Remote Sensing of Environment*, v. 160, p. 15 – 30, 2015. doi: 10.1016/j.rse.2015.02.001

NOVO, E. M. L. M. *et al*. Proposal for a remote sensing trophic state index based upon Thematic Mapper/Landsat images. *Revista Ambiente Água* [online] v. 8, n. 3, p. 65-82, 2013. doi:10.4136/ambi-agua.1229

ODERMATT, D. *et al*. Review of constituent retrieval in optically deep and complex waters from satellite imagery. *Remote Sensing of Environment*, v. 118, p. 116–126, 2012. doi:10.1016/j.rse.2011.11.013

OGASHAWARA, I. *et al*. Re-parameterization of a quasi-analytical algorithm for colored dissolved organic matter dominant inland waters. *International Journal of Applied Earth Observation and Geoinformation*, v. 53, p. 128–145, 2016.

O'REILLY, J. E. *et al*. Ocean color chlorophyll algorithms for SeaWiFS. *Journal of Geophysical Research*, v. 103, n. C11, p. 24937 – 24953, 1998.doi: 10.1029/98JC02160

PALMER, S. C. J.; KUTSER, T.; HUNTER, P. D. Remote Sensing of Environment Remote sensing of inland waters: Challenges, progress and future directions. *Remote Sensing of Environment*, v. 157, p. 1–8, 2015. doi: 10.1016/j.rse.2014.09.021

POPE, R. M.; FRY, E. S. Absorption spectrum (380 – 700 nm) of pure water. II. Integrating cavity measurements, *Applied Optics*, v. 36, n. 33, p. 8710 – 8723, 1997.

RODRIGUES, T. W. P. From oligo to eutrophic inland waters: Advancements and challenges for bio-optical modeling. 142 f. 2017. *Thesis*. (PhD Cartographic Sciences) - Universidade Estadual Paulista, Presidente Prudente, São Paulo. Retrieved from <https://repositorio.unesp.br/bitstream/handle/11449/150315/rodrigues_twp_dr_prud.pdf?sequence=3&isAllowed=y>.

ROESLER, C. S.; PERRY, M. J.; CARDER, K. L. Modeling in situ phytoplankton absorption from total absorption spectra in productive inland marine waters. *Limnology and Oceanography*, v. 34, n. 8, p. 1510 – 1523, 1989.

RUDORFF, B. F. T. *et al*. Studies on the rapid expansion of sugarcane for ethanol production in São Paulo State (Brazil) using Landsat data. *Remote Sensing*, v. 2, p. 1057-1076, 2010. doi:10.3390/rs2041057.

SHEN, M. *et al.* Determination of the Downwelling Diffuse Attenuation Coefficient of Lake Water with the Sentinel-3A OLCI. *Remote Sensing*, v. 9, n. 12, p. 1246, 2017. doi:10.3390/rs9121246

SMITH, W. S.; ESPÍNDOLA, E. L. G.; ROCHA, O. Environmental gradient in reservoirs of the medium and low Tietê River: limnological differences through the habitat sequence. *Acta Limnologica Brasiliensia*, v. 26, n. 1, p. 73–88, 2014. doi:10.1590/S2179-975X2014000100009

SUN, D.Y. *et al*. Specific inherent optical quantities of complex turbid inland waters, from the perspective of water classification. *Photochem. Photobiological Sci.*, v. 11, p. 1299–1312, 2012.

TASSAN, S.; FERRARI, G. M. An alternative approach to absorption measurement of aquatic particles retained on filters. *Limnology and Oceanography*, v. 40, n. 8, p. 1358 – 1368, 1995. doi : 10.4319/lo.1995.40.8.1358

TASSAN, S.; FERRARI, G. M. Measurement of light absorption by aquatic particles retained on filters: determination of the optical path length amplification by the 'transmittance-reflectance' method. *Journal of Plankton Research*, v. 20, n.9, p. 1699-1709, 1998. doi:10.1093/plankt/20.9.1699

TOMING, K. *et al*. Mapping Water Quality Parameters with Sentinel-3 Ocean and Land Colour **i**nstrument imagery in the Baltic Sea**.** *Remote Sensing*, v. 9, n. 10, p. 1070, 2017. doi:10.3390/rs9101070

TUNDISI, J. G. Recursos hídricos no futuro: problemas e soluções. *Estudos Avançados*, v. 22, p. 7–16, 2008.

TUNDISI, J. G.; MATSUMURA-TUNDISI, T. *Limnologia*, 1 ed., São Paulo: Oficina de Textos, 2008.

VIEIRA, M. S., *et al*. Aspectos da química da água e do sedimento do reservatório de Ibitinga (SP). *B. Inst. Pesca*, v. 28, n. 1, p. 77 - 91, 2002.

WATANABE, F. *et al.* Parameterization and calibration of a quasi-analytical algorithm for tropical eutrophic waters. *ISPRS Journal of Photogrammetry and Remote Sensing*, v. 121, p. 28–47, 2016. doi:10.1016/j.isprsjprs.2016.08.009

YANG, W. *et al*. Retrieval of Inherent Optical Properties for Turbid Inland Waters from Remote-Sensing Reflectance. *IEEE Transactions on Geoscience and Remote Sensing*, v. 51, n.6, p. 3761 – 3773, 2013. doi:10.1109/TGRS.2012.2220147

ZHENG, G.; DIGIACOMO, P. M. Uncertainties and applications of satellite-derived coastal water quality. *Progress in Oceanography*, v. 159, p. 45–72, 2017a.

ZHENG, G.; DIGIACOMO, P. M. Remote sensing of chlorophyll-a in coastal waters based on the light absorption coefficient of phytoplankton. *Remote Sensing of Environment*, v. 201, p. 331–341, 2017b.